UCRL-11587

University of California

Ernest O. Lawrence Radiation Laboratory

PHOTOPION PRODUCTION FROM DEUTERIUM NEAR THRESHOLD

Berkeley, California

DISCLAIMER

Rept. submitted for pub. in the
Physical Review.

UCRL-11587

UNIVERSITY OF CALIFORNIA

Lawrence Radiation Laboratory
Berkeley, California

AEC Contract No. W-7405-eng-48

PHOTOPION PRODUCTION FROM DEUTERIUM NEAR THRESHOLD

William P. Swanson, Duane C. Gates, Thomas L. Jenkins,

and Robert W. Kenney

August 5, 1964

PHOTOPION PRODUCTION FROM DEUTERIUM NEAR THRESHOLD*

William P. Swanson,† Duane C. Gates,‡ Thomas L. Jenkins,**
and Robert W. Kenney

Lawrence Radiation Laboratory
University of California
Berkeley, California

August 5, 1964

ABSTRACT

The reactions $\gamma d \rightarrow \pi^- 2p$, $\pi^+ 2n$ were studied near threshold with the Berkeley electron synchrotron. A 4-in. liquid deuterium bubble chamber served as target and detector in a 194-MeV bremsstrahlung beam hardened by about one radiation length of LiH. A total of 1309 π^- and 447 π^+ events was analyzed. The experimental data for the minus-to-plus ratio R were corrected for final-state Coulomb interactions by the method of Baldin, with the results $R = 1.28 \pm 0.13$ for $160\ \text{MeV} < k < 175$ MeV and $\theta^* > 110$ deg (c.m.); $R \geq 1.13 \pm 0.13$ for $152\ \text{MeV} < k < 160$ MeV and $\theta^* < 110$ deg (c.m.). The theory of CGLN, modified by Ball to include the ρ-exchange parameter Λ, predicts $R = 1.28(1 - 0.14\ \Lambda/e)$. This relation was used with our values of R to obtain $\Lambda/e = 0.0 \pm 0.7$ and $\Lambda/e \leq 0.8 \pm 0.7$ for the above two photon energy ranges. The Chew-Low extrapolation technique was used to obtain the value of the squared matrix element a_0^- for the reaction $\gamma n \rightarrow \pi^- p$. It was found to be a satisfactory method to apply to the deuteron for deriving reaction cross sections for free neutrons. We obtain $a_0^- = 27.3 \pm 2.8$ μb/sr at threshold with a slope of -0.30 ± 0.16 μb/sr-MeV. Our most accurate value is $a_0^- = 23.3 \pm 1.9$ μb/sr at $k_{\gamma n} = 162$ MeV. These results have been corrected for the final-state $\pi^- p$ interaction, by means of the Coulomb penetration factor. The threshold

value of the squared matrix element for the reaction $\gamma p \rightarrow \pi^+ n$ was determined to be $a_0^+ = 21.5 \pm 0.9$ μb/sr by McPherson et al. using the same apparatus. Combining these results gives the values $R = a_0^-/a_0^+ = 1.27 \pm 0.13$ at threshold and $\Lambda/e = 0.06 \pm 0.7$. The results are in good agreement with the CGLN theory, and consistent with a value $\Lambda = 0$.

I. INTRODUCTION

The ratio of photopion production from neutrons to that from protons near threshold is a physical quantity of continuing interest. This quantity $R \equiv \sigma^-/\sigma^+ \; \sigma(\gamma n \rightarrow \pi^- p)/\sigma(\gamma p \rightarrow \pi^+ n)$ is important for the following reasons: (a) A firm theoretical prediction has existed since 1957, when the dispersion relations of Chew, Goldberger, Low, and Nambu (CGLN) were published.[1] (b) There is an intimate relationship between R and other measurable pion-nucleon parameters. These parameters are the cross section for positive photopion production by protons near threshold, the pion-nucleon s-wave phase shifts, and the Panofsky ratio. These parameters have been the subject of widespread discussion and controversy.[2-16] (c) Recent corrections to the theory of photopion production have introduced the possibility of detecting the contribution of dipion or ρ-meson exchange terms.[17-25] The value of R is very sensitive to these terms, since they enter in the π^- and π^+ amplitudes with opposite relative signs.

Because of its simple structure, deuterium has been generally used to study negative photopion production, and the σ^-/σ^+ ratio R.[26-45] Most previous experimentation has involved particle-detection techniques using thin targets or deuterium-loaded photographic emulsions. Complete analysis of these experiments was limited because of the incompleteness of kinematic data due to the difficulty of detecting the low-energy pions and recoil nucleons that occur near threshold. In these reactions, the "spectator" nucleon usually recoils with enough momentum to invalidate simple two-body kinematics. Also, unless rather complete kinematic information is available, it is difficult to apply the correction that Baldin has estimated for the final-state Coulomb interaction in the

$\gamma d \rightarrow \pi^- 2p$ reaction.[10]

An alternative approach used by Gatti et al.[46] is to measure the cross section $\sigma(\pi^- p \rightarrow \gamma n)$ and apply detailed balance. This obviates the difficulties inherent in using a deuterium target, but suffers from the difficulties in detecting neutral particles.

In several important respects, a deuterium-filled bubble chamber is an ideal instrument with which to study photopion production by deuterons near threshold: (a) Both negative and positive mesons may be observed simultaneously. (b) The reactions may be studied quite near threshold, because the secondary particles are not required to emerge from the chamber and enter a separate detector. (c) A range of photon energies may be simultaneously studied, yet it is possible to determine accurately the photon energy for each event of the type $\gamma d \rightarrow \pi^- 2p$. (d) Complete kinematic information on this reaction is obtainable, enabling us to make use of the Chew-Low extrapolation technique.

In 1959, Chew and Low[48] described a very powerful method by which cross sections of target particles that are actually bound in a complex system may be analyzed to yield the free-particle cross section. We have used their method to obtain the free neutron cross section $\sigma(\gamma n \rightarrow \pi^- p)$ from observations of negative pion production in a deuterium bubble chamber. This is done by fitting a prescribed function to the measured differential cross section for various values of the spectator proton momentum p_1. Extrapolation of this empirical curve to the (nonphysical) point, where $p_1^2 = -\alpha^2$, yields the free-neutron cross section. The constant α is the deuteron inverse radius.

As may be judged from Fig. 6, the distance of extrapolation is not large compared with the range of values of p_1^2 accessible in the

experiment to be described. Therefore we are able to make a relatively reliable extrapolation.

II. EXPERIMENTAL TECHNIQUE

A. Apparatus and Procedure

Figure 1 shows the arrangement of the apparatus used to produce a clean, "hardened" 194-MeV bremsstrahlung spectrum incident on the 4-in.-diameter liquid deuterium bubble chamber.[49,50] There was approximately one radiation length of LiH between the Pt target of the synchrotron and the bubble chamber. This served to reduce the relative number of photons with energies below the pion production threshold, which contributed only to undesirable electron background in the chamber. Also, thin entrance and exit windows were used on the bubble chamber. Because of the large background of Compton and electron pair-production reactions produced within the chamber by such a beam, it was necessary to operate the chamber in a temperature range such that minimum-ionizing background particles left very tenuous tracks but the slower pions and protons left clearly distinguishable dark tracks. Details of operation and the photon spectrum are presented elsewhere.[51-53] The primary flux monitor for the experiment was a Cornell-type thick-wall ionization chamber placed behind the bubble chamber as shown in Fig. 1. Its calibration[54,55] was corrected to account for the hardened spectral shape and the duty cycle of the bubble chamber operation. The average photon flux through the chamber was 0.8×10^6 MeV per picture. In an auxiliary experiment, a pair spectrometer was used to determine both the peak energy and the spectrum of the bremsstrahlung beam. The synchrotron was operated at peak energies of 194 ± 2 MeV for the main run and 138 ± 1.5 MeV in order

to evaluate background effects. Data collected during the lower-energy run were used to estimate the background subtraction for two- and three-prong photoproton scatterings capable of simulating negative-meson events. The 194-MeV peak energy for the main experiment was selected because, above 180 MeV, chamber efficiency for analyzable pion events dropped rapidly, and higher-energy photons caused ambiguity in interpretation of certain observed events and contributed to the electron background.

Because of the limited track lengths available, the use of a magnetic field would not have facilitated the analysis of this experiment.

B. Measurement and Interpretation of Events

Three hundred thousand stereoscopic photographs were scanned twice, yielding 1309 analyzable π^- events from the reaction

$$\gamma d \rightarrow \pi^- 2p \qquad (1)$$

and 447 events from the reaction

$$\gamma d \rightarrow \pi^+ 2n \qquad (2)$$

(followed by $\pi^+ \rightarrow \mu^+ \nu$).

See Figs. 2 and 3. These events were observed in two separate scans with calculated overall scanning efficiencies of 98.4% and 99.8%, respectively. Measurements from the stereo pictures allowed the spatial reconstruction of each multipronged event and the calculation of the angles and lengths of the tracks.

The main problem in the interpretation of events was the separation of pion events from a background of photonuclear-product scatterings that might simulate the desired pion events. For this reason, the complete analysis of every event included visual inspection of

ionization, as well as kinematical analysis.

The contributing background reactions are $\gamma d \rightarrow \pi^o d$, $\gamma d \rightarrow \pi^o np$, $\gamma d \rightarrow np$, and $\gamma d \rightarrow \gamma d$. The background of single-prong heavy-particle events was about one per frame. We analyzed the photoproton scatterings found in the film exposed at 138 ± 1.5 MeV, exactly as if they were cases of negative photopion production. The visual inspection was done by a physicist unaware of the nature of these events. All these events were identified as photoproton scatterings by the location of the vertex outside of the beam, by the direction of the ionization density gradients of the tracks, or by kinematical analysis.

The π^+ events were identified by the characteristic range of the muon (1.0035 ± 0.053 cm in the bubble chamber), and in 27% of the cases by the electronic muon decay as well. The average range of the muons in visible $\pi^+ - \mu^+ - e^+$ decay chains was used to determine the density of liquid deuterium in the chamber, using the expression

$$\rho_d = \frac{M_d}{M_p} \frac{(\text{muon range in hydrogen, g-cm}^{-2})}{(\text{muon range in deuterium, cm})}$$

$$= \frac{2.01471}{1.00813} \frac{(0.0656 \text{ g-cm}^{-2})}{(1.0035 \text{ cm})} = 0.1307 \pm 0.0013 \text{ g-cm}^{-3},$$

where M_d/M_p is the ratio of the mass of the deuterium atom to the mass of the hydrogen atom. We assumed the muon range in hydrogen to be that given by Clark and Diehl.[56] The range-energy curves of Clark and Diehl were scaled according to our observed muon range. In the region of

interest ($R < 10$ cm) the adjusted range-momentum relationships very closely followed the forms

$$P = 144\ R^{0.277}\ \text{(protons)}, \qquad P = 36.3\ R^{0.270}\ \text{(pions)}, \tag{3}$$

where the momentum P is in MeV/c and the range R is in cm.

By means of energy-momentum conservation equations, it was possible to completely solve any π^- event in which three prongs were visible, and those events in which only two prongs were visible but both prongs stopped in the chamber.

The initial problem was to determine which of the three outgoing particles was the meson and which were protons. To do this, each event was solved completely three times, each time with a different mass selection. An unambiguous choice was usually given by these results. Ten fundamental quantities must be obtained or inferred from the measurements on each event. These are the photon energy k and the three momentum components of each of the three final-state particles. The photon direction was determined separately by measurements on electron pairs in a more sensitive sample of film. At least six of the fundamental quantities must be obtained directly from the measurements and the range-momentum relationship. As many as nine of these quantities were determined directly, if three visible tracks stopped in the chamber. The remaining unknown quantities were obtained by using the four conservation equations for energy and momentum. When more than the necessary six quantities were available from the measurements the problem was overdetermined. A least-squares adjustment to the conservation laws was made by a set of IBM-650 routines that used the method of Lagrange multipliers and an iteration procedure.[57,58] When the adjustment was concluded, the program tested to make sure that the photon energy was reasonable, the event originated in the beam cylinder and within arbitrary fiducial limits, the constraints were sufficiently satisfied,

and χ^2 was reasonable.

III. THE RATIO OF NEGATIVE TO POSITIVE PIONS

A. Pion Energies and Angles Included

In order to be identifiable, a positive pion must stop in the bubble chamber. Therefore, the pion energy range allowed in determining the σ^-/σ^+ ratio R was necessarily limited. We included only pions whose momenta lay between 29 and 51 MeV/c, corresponding to ranges of 0.42 to 3.3 cm. Thus all pions were of sufficiently long range for reliable identification, and still short enough so that positive-pion tracks normally ended in the chamber and their decay signatures were visible.

The data were divided into twenty energy-angle bins to facilitate making geometry and Coulomb corrections. The bins are shown in Fig. 4. The curves that define the bins are based on kinematics of the process $\gamma p \rightarrow \pi^+ n$. If the deuteron binding energy and the neutron-proton mass difference are taken into account, these kinematics fairly accurately represent the kinematics for the process $\gamma d \rightarrow \pi^- p$ + (p at rest), as well as for $\gamma p \rightarrow \pi^+ n$. Two-body kinematics must be used because the $\pi^+ nn$ final state is not amenable to analysis. These curves therefore have only an approximate relationship to our data. The bins were chosen to lie between curves of equal photon energy (lab) and pion c.m. angle, so that the ratio R could be studied as a function of these variables. Areas that were too small to efficiently serve as bins were arbitrarily made part of an adjacent bin in the same energy region.

The dashed line running almost vertically through Fig. 4 divides the data into two regions. To the right of this line (forward direction), a negative pion is capable of carrying so much forward momentum that both

protons may be of invisibly short range. The ratio R obtained in this forward region must be interpreted as a minimum value. To the left of this line, however, at least one proton and the negative pion always have a visible range ($R > 1.0$ mm) and any final state of the $\pi^- pp$ system is observable in this energy-angle region.

B. Positive Pions

It is clear that positive pions produced in the bubble chamber may be close enough to the chamber wall to escape, even though their momentum falls in the range accessible to our analysis. To account for these lost events, each detected event was weighted by an IBM-7094 Monte Carlo routine. This routine randomly displaced and reoriented each event repeatedly, each time testing to see whether it remained entirely within the chamber.

The routine gave each event successive random positions until 100 analyzable positions had been counted. The weight of the event was given by the ratio of the total number of positions tested to the number of detectable positions found. The boundaries in pion momentum of Fig. 4 never allowed the escape correction factor to exceed about 2.0 in any bin. The statistical error due to the Monte Carlo procedure is negligible. Other corrections to the π^+ data are as follows:

Scanning efficiency	+ 0.2%,
H^1 impurity	- 1.0%,
Muon range not acceptable	+ 0.01%,
Pion decay in flight	+ 1.2%.

The net correction was judged to be negligible. Errors other than the statistical error were also assumed to be negligible. The number of acceptable positive pion events found was 291.

C. Negative Pions

Analysis of the negative pions was complicated both by final-state Coulomb corrections, and by corrections for chamber geometry. The corrections for chamber geometry were made in the following way. All those events that had one proton of invisibly short range were weighted by an IBM-7094 Monte Carlo routine similar to the one used to weight the positive pion events.

Three-prong events were included in the data only if they occurred in regions of the chamber wherein all three-prong events that were similar in pion momentum and angle would be analyzable. The boundaries of these regions are functions of the momenta of the particles involved. It was possible to simplify the problem by dividing the acceptable pion angle-momentum area of Fig. 4 into three regions, each of which accepted three-prong events from various portions of the chamber, subject to certain photon-energy restrictions.

In the long horizontal region above the light line near the top of Fig. 4, the pion has enough momentum to leave the chamber, if produced in certain regions. Three-prong events having a leaving pion track are detectable with full efficiency only if the longest-range proton possible is always visible. Certain restrictions on the position of the vertex were made to insure that this condition was always satisfied. Different restrictions were applied to the small wedge-shaped region above the shorter light line at the extreme right, and to the remaining area below the light lines.

Weights were given to the events satisfying these restrictions, in order to account for those missed in the remaining portions of the chamber. These weights were simply the ratio of "standard" chamber path length (7.0 cm) to accepted chamber path length.

Other corrections to the π^- data are as follows:

Scanning efficiency	1.6 ± 1.6%
Events difficult to measure	4.0 ± 2.5%
Net correction	5.6 ± 3.0%

The raw number of negative pion events included in our analysis was 376.

D. Coulomb Corrections

A positive correction (around 5% in our energy region) is required because the pp final-state Coulomb repulsion tends to reduce the overall production cross section. Of course the pp s-wave nuclear interaction strongly affects the cross section as well. However, a similar nn final state interaction in positive photopion production approximately cancels the effect of the pp nuclear interaction when the σ^-/σ^+ ratio is obtained.

Using the impulse approximation, Baldin[10] has calculated the effect of the pp final-state Coulomb interactions. He found the differential cross section $\frac{\partial^2\sigma}{\partial p \partial q}$ for negative photopion production from deuterium near threshold to be approximately equal to $A(p,q)|K^-|^2$, in the absence of Coulomb interaction. The variables p and q are half the magnitudes of the vector sum and difference of the final-state proton momenta, respectively:

$$p = \left|\frac{\underset{\sim}{p}_1 - \underset{\sim}{p}_2}{2}\right|, \qquad q = \left|\frac{\underset{\sim}{p}_1 + \underset{\sim}{p}_2}{2}\right|.$$

Also, $|K^-|^2$ is the spin-flip matrix element squared for negative photopion production from free neutrons. Baldin also used exact pp Coulomb final-state wave functions to calculate coefficients $A^c(p,q)$ to replace the $A(p,q)$.

We used Baldin's tabulated values of $A(p,q)$ and $A^c(p,q)$, and individually weighted each event found by the ratio (A/A^c). The values

used appear in Table I.

A negative correction (around 15% in our data) is also required because the final-state Coulomb attraction between pion and proton tends to increase the overall cross section. To correct for this effect we used an approximation to the Coulomb "penetration factor"[59] along lines suggested by Baldin.[10] Each event was weighted by the quantity

$$C^2 \approx 1 - \pi e^2 \left(\frac{1}{v_1} + \frac{1}{v_2}\right) \quad , \qquad (4)$$

where v_1 and v_2 are the velocities of the pion measured with respect to each of the outgoing protons, respectively, in the c.m. of pion and proton.

This use of the Coulomb penetration factor is not entirely correct, since it is appropriate only for boson emission from a single nucleon. In our case, we have two protons, either of which may have emitted the pion. Since we have no reason to prefer one proton over the other, we include them both in Eq. (4) on an equal basis. This formula then corrects for the emitting or parent nucleon in a proper manner through one of its terms. The other term is not exactly correct, but we believe that its effect is in the right direction to correct for the effect of the nonemitting proton. The error introduced through its use should not be serious.

E. Results

Table I summarizes the analysis and results of our determination of R, as directly observed in the deuterium bubble chamber. The raw and corrected numbers of events are tabulated as a function of the laboratory-system photon-energy and c.m.-angle bins shown in Fig. 4. Two-body kinematics for the reaction $\gamma p \rightarrow \pi^+ n$ were used in choosing the bins, as

explained above. The pp Coulomb corrections, the π^-p Coulomb corrections, and the geometry corrections shown were determined by the methods just described.

In the right-hand part of Table I, the data for the six energy bins were combined, and the value of R is given for each of the energy bins, I-IV. The 5.6% correction in the negative pion data for scanning efficiency and measurement difficulties (explained above) was applied at this point. Therefore the values for R are the corrected number of negative pions times the factor (1.056 ± 0.030) divided by the corrected number of positive pions.

Note that the three values of R for energy bins I, II, and IIIA-IIIC are minimum values, because full negative pion detection efficiency is not assured in this region, and a method of correcting for missing events having both proton tracks shorter than 1.0 mm was not found. However, the values of R for the higher-energy bins III D - III F, IV, V, and VI represent the true value of R, within the experimental error.

In the final column of Table I, the values of R are given, averaged over the region not fully amenable to correction, and over the region in which all known corrections may be calculated, respectively. The important conclusions from this analysis are that

$$R \geq 1.13 \pm 0.13$$

for the region roughly defined as

$$152 \text{ MeV} < k_{lab} < 160 \text{ MeV}, \text{ and } \theta_{c.m.} < 110 \text{ deg},$$

and $R = 1.28 \pm 0.13$ in the region roughly defined as

$$160 \text{ MeV} < k_{lab} < 175 \text{ MeV}, \text{ and } \theta_{c.m.} > 110 \text{ deg}.$$

To check on the validity of the use of two-body kinematics to

determine the average photon energy, we examined the distribution of true photon energies of the negative meson events used in Table I to determine the ratio R. The graphs of Fig. 5 show the number of events, after Coulomb and geometry corrections, as a function of the algebraic difference between the true laboratory-system photon energy, and the photon energy obtained from two-body kinematics for the process $\gamma p \rightarrow \pi^+ n$.

The three histograms contain events with pion lab momentum and angle in the ranges given in the caption. These groupings are approximately equivalent to dividing the data into three groups containing events from bins I and II, Bin III, and bins IV through VI of Fig. 4, respectively.

The distributions are each peaked at about zero, meaning that the most probable true photon energy is correctly given by two-body kinematics. However, each distribution has a high-energy tail which makes an important contribution. Kinematic limitations restrict the number of lower-energy events, and explain the skewness of the distributions.

IV. THE CHEW-LOW EXTRAPOLATION

A. The Extrapolation Procedure

The cross section for the process $\gamma n \rightarrow \pi^- p$ on free neutrons is obtained by means of the expression[48]

$$G(p_1^2, w^2, k) = \frac{4\pi k^2}{r^2} \left(\frac{M_d}{M_p}\right)^2 \frac{\left(p_1^2 + \alpha^2\right)^2}{\left(w^2 - M_n^2\right)} \frac{\partial^2 \sigma}{\partial^2 p_1^2 \partial w^2} , \qquad (5)$$

where p_1 is the spectator proton momentum, w is the total c.m. energy of the $\pi^- p$ system, and k is the synchrotron photon laboratory-system energy. The ranges of p_1^2 and w^2 allowed by kinematics are shown in Fig. 6 as a function of k. M_d, M_p, and M_n are the rest masses of the deuteron, proton, and neutron, respectively, and α is the inverse deuteron

radius. For convenience, the symbols used in this section are summarized in Table II ($\hbar = c = \mu = 1$).

The constant Γ^2 contains only np interaction parameters and is given by

$$\Gamma^2 = \frac{4}{M_p} \frac{\alpha}{1 - \alpha r_{0t}}, \tag{6}$$

where r_{0t} is the neutron-proton triplet effective range.[60]

The cross section $\sigma(\gamma n \to \pi^- p)$, at a laboratory-system photon energy

$$k_{\gamma n} = \frac{w^2 - M_n^2}{2M_n}, \tag{7}$$

is given by the limit

$$\sigma(\gamma n \to \pi^- p) = \lim_{p_1^2 \to -\alpha^2} G(p_1^2, w^2, k).$$

In the foregoing discussion, it has been assumed that the spectator nucleon is well defined. A better way of formulating the problem is to deal with a scattering amplitude $f(p_1,p_2)$ which is symmetric in the final-state laboratory-system momenta, p_1 and p_2, of the two nucleons and which has a first-order pole in the square of the nucleon momentum located at $-\alpha^2$.

Suppressing all variables but these two momenta, p_1 and p_2, one can write this amplitude

$$f(p_1,p_2) = \frac{g(p_2)}{p_1^2 + \alpha^2} + g'(p_1,p_2) + \frac{g(p_1)}{p_2^2 + \alpha^2} + g'(p_2,p_1),$$

where g represents the pole contribution to the amplitude and the g' are terms that are less singular than the pole terms and therefore unimportant in the limit of $p_1^2 = -\alpha^2$. The cross section of interest is then

proportional to $\lim_{p_1^2 \to -\alpha^2} |f(p_1,p_2)|^2$.

The experimental data for a given value of p_1 may be analyzed by including events of all $p_2 > p_1$. A tabulation of the data which uses this choice of recoil momenta is designated "Table A" in Sec. IV.E and in Table III. The cross section can be written as an integral over p_2:

$$\frac{\partial^2\sigma}{\partial p_1^2 dw^2} = \int_{p_1}^{\infty} |f(p_1,p_2)|^2 \, dp_2 = \frac{H}{\left(p_1^2 + a^2\right)^2} + \text{less singular terms.}$$

We might, on the other hand, arbitrarily choose p_1 to be the higher recoil momentum. Experimentally we then include all recoil momenta p_2 for a given p_1, where $p_2 < p_1$; p_1 is still the extrapolation variable. The cross section may then be written similarly:

$$\frac{\partial^2\sigma}{\partial p_1^2 \partial w^2} = \int_{0}^{p_1} |f(p_2,p_1)|^2 \, dp_2 = \frac{H'(p_1)}{(p_1^2 + a^2)^2} + \text{less singular terms.}$$

As $p_1^2 \to -a^2$, the integral vanishes in the physical region in the neighborhood of $p_1 = 0$ because the limits of integration approach each other. Then $\frac{d^2\sigma}{dp_1^2 dw^2}$ must be near zero at $p_1^2 = -\alpha^2$ and therefore this choice of recoil, designated "Table B" in our data library, gives a small value for the extrapolated cross section.

It is therefore allowable either to use Table A alone, or alternatively to use each event twice in a single extrapolation. In the latter case one includes both choice A and choice B for each event. This is designated "Table A + B."

For convenience in using the maximum-likelihood method described below, $G(p_1^2, w^2, k)$ is expressed as

$$G(p_1^2, w^2, k) = 4\pi W(w^2) \left[A_0 + A_1(w^2 - w_0^2)\right] + (p_1^2 + \alpha^2) \left[A_2 + A_3(k - k_t) + A_4(w^2 - w_0^2)\right] , \quad (8)$$

where the A's are adjustable parameters.

This expression may be analyzed in the following way. At the limit ($p_1^2 = -\alpha^2$), the desired cross section has the simple form given by the leading term in Eq (8),

$$\sigma(\gamma n \to \pi^- p) = 4\pi\, W(w^2) \left[A_0 + A_1(w^2 - w_0^2)\right] . \quad (9)$$

The expression for the cross section (Eq. 8) should depend only on w^2. Provision is made for such dependence through the parameters A_0 and A_1, and the phase space factor $W(w^2)$, which has been defined by Beneventano et al.,[35]

$$W(w^2) = \frac{p_\pi^* \omega}{\left(1 + \frac{\nu}{E_i}\right)\left(1 + \frac{\omega}{E_f}\right)} , \quad (10)$$

where p_π^*, ω, ν, E_i, and E_f are respectively the pion momentum, pion total energy, photon momentum, initial nucleon total energy, and final nucleon total energy. These quantities are all functions of w^2, and are defined in the γn center of mass. Except where noted, $\hbar = c = \mu = 1$.

The use of $W(w^2)$ in the above equations is equivalent to equating $[A_0 + A_1(w^2 - w_0^2)]$ to a_0^-, the matrix element squared defined by Benventano et al. Furthermore, A_0 is equal to the threshold ($w^2 = w_0^2$) value of a_0^-. This parameter is the one of greatest physical interest in this

analysis. The implicit assumption in the equation

$$\sigma(\gamma n \to \pi^- p) = 4\pi\, W(w^2)\, a_0^- \qquad (11)$$

is that the differential cross section is isotropic in the range of w^2 included in this experiment. This is true because at values of w^2 near threshold, there is little energy available for angular momentum states higher than s-wave. This has been experimentally verified in work on positive photopion production.[61-73]

The form of Eq. (8) was limited to first order in p_1^2, w^2, and k. Higher-order terms could have been included, but we felt that the data were not sufficient to determine more parameters.

B. Application of the Maximum-Likelihood Method

It is well known that the maximum likelihood method uses a given set of data in the most efficient way possible. The maximum likelihood method was used in preference to a least-squares fit, because when the data were divided into three-dimensional bins in p_1^2, w^2, and k, the statistics in each bin were often so poor as to prevent a meaningful fit in p_1^2, particularly where the range in p_1^2 was kinematically limited. Furthermore, the complicated shape of the kinematical limits in p_1^2, w^2, and k make binning an awkward procedure. (See Fig. 6.) For these reasons we felt that the maximum likelihood method was ideally suited to our analysis.

In order to employ the maximum-likelihood method,[74] one may use a general parameterized expression $P(A_0, A_1, \cdots, A_m, X_0, X_1, \cdots, X_n)$ that represents the differential probability of having an event occur at coordinates (such as angle, energy, etc.) $X_0, X_1, \cdots, X_n$. The quantities $A_0, A_1, \cdots, A_m$ are parameters of the theory for the effect studied. They are to be varied until a maximum is found in the "overall probability" for having obtained the experimental results actually obtained.

In our experiment, $\underset{\sim}{A} = (A_0, A_1, \cdots, A_4)$ is the set of parameters of Eq. (8) and $\underset{\sim}{X} = (p_1^2, w^2, k)$ is the set of experimental variables.

The "overall probability" is commonly called the likelihood function $\mathcal{L}$ and may be written

$$\mathcal{L} = \prod_i P(\underset{\sim}{A}, \underset{\sim}{X}) \cdot \exp\left(- \int P(\underset{\sim}{A}, \underset{\sim}{X}) d\underset{\sim}{X} \right) . \qquad (12)$$

The product $\prod_i P$ is the product of individual probabilities for producing the actual events seen. The exponential may be thought of as

the probability of events' being absent in regions of the experimental variables $\underset{\sim}{X} = (p_1^2, w^2, k)$ where events did not occur (see reference 74, for example).

The probability of seeing an event produced at $\underset{\sim}{X} = (p_1^2, w^2, k)$ is

$$P(p_1^2, w^2, k) = C_c(p_1^2, w^2, k) \times E(p_1^2, w^2, k) \times S(k) \times Nt \frac{\partial^2 \sigma}{\partial p_1^2 \partial w^2} =$$

$$C_c(p_1^2, w^2, k) \times E(p_1^2, w^2, k) \times S(k) \times Nt \frac{\Gamma^2}{4\pi k^2} \left(\frac{M_p}{M_d}\right)^2 \frac{\left|w^2 - M_n^2\right|}{\left|p_1^2 + \alpha^2\right|^2} G(p_1^2, w^2, k) \tag{13}$$

$$= \frac{1.7527}{k^2} C_c(p_1^2, w^2, k) \times E(p_1^2, w^2, k) \times S(k) \frac{\left|w^2 - M_n^2\right|}{\left|p_1^2 + \alpha^2\right|^2} G(p_1^2, w^2, k).$$

As defined by Eq. (7), $G(p_1^2, w^2, k)$ is inserted in the right-hand side of this expression; $C_c(p_1^2, w^2, k)$ is a correction for the final-state Coulomb interaction between particles. It is discussed in Sec. IV. D. The $E(p_1^2, w^2, k)$ is an instrumental efficiency function. It is the probability of detecting an event in the bubble chamber with variables (p_1^2, w^2, k) if such an event is produced. Its calculation is discussed in Sec. IV. C. $S(k)$ is the spectrum function which gives the number of incident synchrotron photons per 1-MeV energy interval. Since pion units ($\hbar = c = \mu = 1$) are otherwise used throughout, $S(k)$ determines the units of P to be MeV^{-1}. $N = \rho N_0/A$ is the number of deuterons per cubic centimeter, and t is the target path length available.

C. Calculation of Geometric Detection Efficiencies

In order to perform the Chew-Low extrapolation by means of a maximum-likelihood method it is necessary to write an expression (Eq. 13)

for the probability of observing an event with particular values of p_1^2, w^2, and k. This expression contains, besides the cross section, the detection efficiency $E(p_1^2,w^2,k)$ for recognizing the event in the bubble chamber. Since the values of p_1^2,w^2, and k do not uniquely determine the configuration of an event, it was necessary to average over two other parameters in order to calculate an average geometrical efficiency for a particular value of p_1^2,w^2, and k. The parameters chosen for this averaging procedure were the polar and azimuthal angles of emission of the pion in the center of mass system of the pion and non-spectator proton.

A computer program calculated these average efficiencies for a particular set of p_1^2,w^2, and k by generating the laboratory angles and ranges for the three particles over the possible range of c.m. angles. Each "event" so generated was assigned a detection efficiency. The detection efficiency was set equal to unity if all three tracks would have been visible in the chamber. If only two tracks would have been visible, then a Monte Carlo calculation was made to determine the probability that this event would be so located in the chamber that both tracks were seen stopping. This calculation consisted of placing the vertex of the "event" at randomly chosen positions throughout the fiducial volume. At each position it was determined whether or not the ends of the tracks remained within the chamber. The ratio of events lying within the chamber to the total events tried was then taken as the detection efficiency. In this manner, a table of average efficiencies $E(p_1^2,w^2,k)$ for various values of p_1^2, w^2, and k was then used as input to the maximum-likelihood calculation.

D. Coulomb Corrections

The cross section for the reaction $\gamma d \to \pi^- 2p$ is affected by the pp nuclear interaction, as well as Coulomb interactions between all pairs of final-state particles. By extrapolating Eq. (8) to $p_1^2 = -\alpha^2$, we eliminate the effects of these interactions. (An exception is the interaction between the pion and the parent nucleon. A correction for this remaining interaction may be made, using the Coulomb penetration factor.)[59] Nevertheless, it is desirable to correct for these effects in the physical region, in order to make the extrapolating curve as smooth as possible.

The correction factor $F(\underset{\sim}{p}_1, \underset{\sim}{p}_2, w^2)$ that we used was the ratio of the cross section for the event, as calculated in the impulse approximation including the final-state interactions, to the cross section as calculated for the neutron-exchange diagram alone. (The lab momenta $\underset{\sim}{p}_1$ and $\underset{\sim}{p}_2$ are the momenta of the protons assumed to be the spectator and the parent, respectively.) If the impulse approximation were exact, the resulting extrapolation curve would be constant. Although not exact, the impulse model does reproduce the main features of the cross section,[10] and the extrapolation curve should be nearly flat. An indication of the correctness of this procedure is provided by the values of the parameters A_2, A_3, and A_4, which determine the flatness of the extrapolation curve. (See Table III.)

The impulse approximation was calculated by Schult,[47] using the method of Baldin,[10] and gave the expression

$$F(\underset{\sim}{p}_1, \underset{\sim}{p}_2, w^2) = (p_1^2 + \alpha^2)^2 \left\{ \frac{2}{3} \left| J_1(\underset{\sim}{p}_1) - J_1(\underset{\sim}{p}_2) \right|^2 + \frac{1}{3} \left| J_1(\underset{\sim}{p}_1) + J_1(\underset{\sim}{p}_2) + 2 f_s(p)\, J_2(p,q) \right|^2 \right\} C^2(\eta)\, C^2(\eta_\pi). \tag{14}$$

The expressions entering Eq. (14) are:

$$J_1(\underset{\sim}{p}_1) = \frac{\exp\left[\eta \tan^{-1} 2p\alpha/(\alpha^2 + q^2 - p^2)\right]}{(p_1^2 + \alpha^2)} \exp\left[i \frac{\eta}{2} \ln \frac{(\alpha^2 + q^2 - p^2)^2 + 4p^2\alpha^2}{(p_1^2 + \alpha^2)^2}\right] - \frac{0.043}{\alpha^2} ,$$

$$J_2(p,q) = \frac{i}{2qc^2(\eta)} \int_0^1 t^{i\eta} \left[\frac{1}{t + \frac{p - q + i\alpha}{p + q - i\alpha}} - \frac{1}{t + \frac{p + q + i\alpha}{p - q - i\alpha}}\right] dt - \left(\frac{0.27\alpha + 0.043ip}{\alpha^2 c^2(\eta)}\right),$$

$$f_s(p) = \frac{e^{i\delta(p)} \sin \delta(p)}{p} ,$$

$$p = \left|\frac{\underset{\sim}{p}_1 - \underset{\sim}{p}_2}{2}\right|, \quad q = \left|\frac{\underset{\sim}{p}_1 + \underset{\sim}{p}_2}{2}\right|, \quad c^2(\eta) = \frac{2\pi\eta}{e^{2\pi\eta} - 1} , \quad \eta = \frac{e^2}{\hbar} \frac{M}{2p} ,$$

$$\eta_\pi = \frac{-e^2}{\hbar} \frac{\mu}{p_\pi^*(1 + \mu/M)} ,$$

where $\alpha = 0.3274$ is the deuteron inverse radius, M is the nucleon mass, δ is the pp s-wave scattering phase shift, p_π^* is the momentum of the pion in the c.m. of the pion and parent nucleon, and μ is the pion mass ($\hbar = c = \mu = 1$).

The first term within braces in Eq. (14) contains the impulse integrals for photopion production leading to a nucleon-nucleon spin-triplet final state. The second term contains analogous expressions for the nucleon-nucleon spin-singlet final state. The pp s-wave nuclear interaction enters the second term through the scattering phase shift $\delta(p)$. The relative weights 2/3 : 1/3 are obtained, if the spin-flip matrix element is assumed to dominate in this energy region. The terms $\frac{0.043}{\alpha^2}$, and $\frac{0.27\alpha + 0.043\, ip}{\alpha^2\, c^2\, (\eta)}$ are intended to remove contributions to the impulse integrals from the region $r < \mu^{-1}$, as suggested by Baldin.

The integral in $J_2(p,q)$ was evaluated numerically in the interval

$\exp(-\pi/2\eta) < t < 1$. The portion of the integral between $t = 0$ and $t = \exp(-\pi/2\eta)$ is negligible for the values of p available in this experiment.

The final multiplicative factor in Eq. (14) corrects for the Coulomb interaction between pion and parent nucleon[59] and is a function of w^2 only.

The Coulomb correction was actually introduced into Eq. (13) by means of a table of values of $C_c(p_1^2, w^2, k)$. These quantities are values of $F(\underset{\sim}{p}_1, \underset{\sim}{p}_2, w^2)$, averaged over the pion angles, as described in the preceding section (IV.C).

E. Details of the Maximum-Likelihood Calculation

The maximum-likelihood calculation discussed in Sec. IV.B was performed on an IBM computer. Input to the program consisted of the p_1^2, w^2, and k parameters for each event. To each event could be assigned two sets of w^2 and p_1^2, because each proton could in turn be considered as the spectator. That set of data in which the lower-energy proton was considered to be the spectator was designated Table A, that in which the higher energy proton was considered to be the spectator was designated Table B. Besides the event data, a table of efficiencies covering the range of p_1^2, w^2, and k used was provided as input. This table included either the geometric efficiency described in Sec. IV. C, or final-state interaction "efficiency" described in Sec. IV. D, or both.

A subroutine of the program was capable of calculating the natural logarithm of the likelihood function $\ln \mathcal{L}$, defined in Sec. IV.B, for arbitrary values of the A_i parameters. This calculation was done in two steps. First, a numerical integration of $P(\underset{\sim}{A}, \underset{\sim}{X})$ was performed over the region of interest by applying Simpson's rule to a 9 by 9 by 9 array

of points throughout the volume of interest. Second, a sum of the logarithms of the $P(\underset{\sim}{A},\underset{\sim}{X})$ for the individual events was formed.

The maximizing process consisted of varying $\underset{\sim}{A}$ until a maximum in $\ell n\,\mathcal{L}$ was found. This was accomplished in two steps. First, $\ell n\,\mathcal{L}$ was calculated for a range of arbitrary values of each component of $\underset{\sim}{A}$ and the approximate region where $\ell n\,\mathcal{L}$ is maximum was located. Then, starting with an $\underset{\sim}{A}$ in this region, the calculation of $\underset{\sim}{A}$ and $\ell n\mathcal{L}(\underset{\sim}{A})$ was put under the control of a subroutine which sought the point of maximum $\ell n\,\mathcal{L}$. This was done by calculating the direction of the gradient $\underset{\sim}{\nabla}(\ell n\mathcal{L})$, in the parameter space of $\underset{\sim}{A}$. Then $\underset{\sim}{A}$ was caused to move in the direction of this gradient until a maximum in $\ell n\,\mathcal{L}$ was found. The point of maximum $\ell n\,\mathcal{L}$ was then used as a new basic point for calculating $\underset{\sim}{\nabla}(\ell n\mathcal{L})$, and the procedure was continued until the distance moved in the parameter space between successive maxima fell below some predetermined small value. The points of maximum $\ell n\,\mathcal{L}$ so determined are given in Table III.

In order to ensure that the maximum $\ell n\,\mathcal{L}$ determined by this procedure was unique, $\ell n\,\mathcal{L}$ was also calculated at arbitrary points on a five-dimensional grid that extended over reasonable values of the parameters. No behavior was seen that suggested the presence of other maxima comparable in height to the one found by the gradient method.

Throughout the calculations, the region in p_1^2, w^2, and k space used was the shaded region shown in Fig. 6. In addition to the kinematic limits, the photon energy k was limited to lie between 150 and 185 MeV, the limits on w^2 were 60.0 to 63.5, and p_1^2 was limited to the interval 0.0 to 1.5. In addition, data lying between the shaded volume and the $k - w^2/\mu^2$ plane were not used. The equation of the plane separating these two regions is

$$1360 - k_{MeV} - 20\,\frac{w^2}{\mu^2} + 200\,\frac{p_1^{\,2}}{\mu^2} = 0.$$

Within these limits the geometrical and Coulomb correction factors remained reasonably close to unity (within a factor of two), and an interpolation could be made with sufficient accuracy.

F. Results of the Extrapolation

The extrapolation of the surface defined by Eq. (5) to $p_1^{\,2} = -\alpha^2$ gives both the threshold value of the matrix element squared and information on its energy dependence.

The agreement between the experimental threshold pion parameters of this work and the CGLN theory, corrected for ρ exchange, gives additional confirmation of the theoretical results near threshold. It is particularly important to note the successful application of the Chew-Low extrapolation technique to deuteron data in deriving cross sections for free neutron targets. Here the interaction amplitude is dominated by a single isolated pole, rather close to the physical region, with no singularities intervening in the extrapolation interval $-\alpha^2 < p_1^{\,2} < 0$. Data are obtained relatively close to the nonphysical region in $p_1^{\,2}$ and the distance of the extrapolation is small (approximately 1 MeV spectator recoil energy) in comparison with extrapolations involving ππ interactions.[75] Extrapolation experiments to obtain information on the ππ coupling constant have encountered difficulties, chiefly because the pole of interest in the scattering amplitude is located much deeper in the nonphysical region and also is in the proximity of other complicating singularities. The closest complicating singularity for our deuteron case involves the pion mass and is located at roughly $p_1^2 = -(\mu/\text{B.E.})\alpha^2$. The effect of this singularity on the scattering amplitude is negligible at $p_1^2 = -\alpha^2$. Consequently, extrapolations to $p_1^2 = -\alpha^2$ involving deuteron data are

expected to be relatively reliable. Our more favorable circumstances have allowed us to measure the cross section for the reaction $\gamma n \rightarrow \pi^- p$ between photons and free neutrons.

A total of 565 events found within the limits described in Sec. IV.E was used in the analysis.

Table III contains best values for the parameters in Eq. (8). This surface was fitted to the data under the three assumptions, Table A, Table B, and Table A+B, previously defined. For each choice, the appropriate geometrical corrections were used (see Sec. IV.E). The column headed "Table A+B" gives the results of this experiment. Table A and Table B are shown for comparison. Table A+B was arbitrarily chosen in preference to Table A because it resulted in a smaller error in A_0, and in an extrapolation surface with less average slope in $(p^2 + a^2)$.

These results show that A_0, the threshold value of the squared matrix element, derived from Table A is equal to that found from Table A+B, within statistics. Furthermore, A_0 found from Table B alone is statistically consistent with zero. This confirms that the extrapolation may be made either by using the momentum of the lower-energy proton as the extrapolation variable p_1, or by using both proton momenta. The use of the momentum of the higher-energy proton alone should lead to an extrapolated cross section consistent with zero, as explained in Sec. IV.A. The 4% difference between the values of A_0 determined from Table A and Table A+B gives a rough indication of the accuracy of this extrapolation technique.

An indication of the correctness of the Coulomb correction (Sec. IV.D) is the fact that the coefficients A_2, A_3, and A_4 are consistent with zero for Table A+B.

The parameter A_0 is exactly the threshold value of a_0^- (see Eq. 11) in units of μb/sr, and its best value, 25.9 ± 2.6 μb/sr, is given in Table III. An additional correction factor (1.056 ± 0.03) explained in

Section III.C, and a normalization uncertainty of ± 4% due to the photon beam monitor must be taken into account. The corrected value is $a_0^- = 27.3 \pm 2.8$ μb/sr. This value does not include any estimate of the uncertainty inherent in the extrapolation technique. It does include a Coulomb correction for the $\pi^- p$ final state interaction based on the Coulomb penetration factor[59] inserted as the last factor in Eq. (14).

The energy dependence of a_0^- is given in terms of the lab energy $k_{\gamma n}$ of the photon involved in the reaction $\gamma n \to \pi^- p$. From Eq. (7), w^2 is substituted in Eq. (8) giving $a_0^- = A_0 + A_1(M_n^2 + 2k_{\gamma n} M_n - w_0^2)$. The slope of a_0^- is $da_0^-/dk_{\gamma n} = 2A_1 M_n$. Our experimental value is given in Table III, and shown in Fig. 8. The final value, corrected by the factor (1.056 ± 0.03) is -0.30 ± 0.16 μb/sr-MeV.

Figure 7 shows the behavior of $\ln \mathcal{L}$ for variations of each single parameter.

An error matrix G_{ij} (Reference 74, p. 15) for the parameters was numerically calculated, assuming

$$< \Delta A_i \, \Delta A_j > = G_{ij} \quad ,$$

where G_{ij} is defined by

$$G_{ij}^{-1} = - \frac{\partial^2 (\ln \mathcal{L})}{\partial A_i \partial A_j} \quad .$$

This matrix is shown in Table IV. The confidence bands on Fig. 8 were calculated by using the relationship

$$(\Delta a_0^-)^2 = \left(\frac{\partial a_0^-}{\partial A_0}\right)^2 <(\Delta A_0)^2> + 2 \frac{\partial a_0^-}{\partial A_0} \frac{\partial a_0^-}{\partial A_1} <\Delta A_0 \Delta A_1> + \left(\frac{\partial a_0^-}{\partial A_1}\right)^2 <(\Delta A_1)^2>,$$

where

$$\frac{\partial a_0^-}{\partial A_0} = 1$$

and

$$\frac{\partial a_0^-}{\partial A_1} = (M_n^2 + 2k_{\gamma n} M_n - w_0^2) = 2M_n(k_{\gamma nt} - k_{\gamma n}) ,$$

where $k_{\gamma nt}$ is the threshold value of $k_{\gamma n}$. The results of these formulas were then quadratically added to the 3% uncertainty due to the correction factor mentioned above, and to the 4% uncertainty in beam monitor calibration.

As may be seen on Fig. 8, the results agree with the uncorrected theory of CGLN in the energy range from threshold to $k_{\gamma n}$ = 189 MeV, or w^2 = 63.5, the highest photon energy allowed in the extrapolation. The uncertainty in a_0^- is least at about $k_{\gamma n}$ = 162 MeV. Here the value of a_0^- is 23.3±1.9 μb/sr, corrected by the Coulomb penetration factor.

V. CONCLUSIONS

The minus-to-plus ratio R was determined in this experiment by observation of both negative and positive photopions produced in deuterium.[76] The Coulomb corrections of Baldin were used to correct for final-state Coulomb interactions. These corrected ratios are in good agreement with the results of other workers,[26-46] and with the dispersion relations of CGLN. The results of this experiment are shown in Fig. 9, together with the data from other experiments, and the theory of CGLN. Limitations in determining R in this manner are the uncertainty in the Coulomb corrections and in the determination of the photon energy.

The value of R depends sensitively on Λ/e, the ρ-exchange parameter, but is only weakly dependent on $N^{(-)}$, a parameter defined by CGLN. This dependence is shown in CGLN's expression for the threshold value of R, modified by Ball's correction[17]

$$R = \left\{\left[1 + (g_p + g_n)(\mu/2M) + 1.15\ N^{(-)}\right]\Big/\left[1 - (g_p + g_n)(\mu/2M) + 1.15\ N^{(-)}\right]\right\}^2$$

$$\times\ (1 - 0.14\ \Lambda/e) = 1.28\ (1 - 0.14\ \Lambda/e).$$

From our experimental values of R given in Table I, this expression yields $\Lambda/e = 0.0 \pm 0.7$ for $R = 1.28 \pm 0.13$ and $\Lambda/e \leqslant 0.8 \pm 0.7$ for $R \geqslant 1.13 \pm 0.13$.

As an alternative means of studying negative photopion production by neutrons, we have applied the Chew-Low extrapolation technique to our data.[77] Table III and Fig. 8 give the extrapolation results. Our value $a_0^- = 27.3 \pm 2.8$ μb/sr at threshold, corrected by the Coulomb penetration factor, is in agreement with the results of Adamovich et al.[15] and with the theory of CGLN. The measured energy dependence of a_0^-, averaged from threshold to $k_{\gamma n} = 189$ MeV, is $da_0^-/dk_{\gamma n} = -0.30 \pm 0.16$ μb/sr-MeV, also in agreement with the results of CGLN.

The threshold value of $a_0^- = 27.3 \pm 2.8$ μb/sr depends on Λ/e and $N^{(-)}$, as well as on f^2, the pion-nucleon coupling constant. Assuming $f^2 = 0.08$ and $N^{(-)} = 0.04 \pm 0.04$,[78] we obtain $\Lambda/e = 1.9 \pm 1.8$. The uncertainties in a_0^- and $N^{(-)}$ contribute about equally to the uncertainty in this determination of Λ/e.

Alternatively, we may compare our threshold value of a_0^- with recent experiments on positive photopion production in hydrogen. The data of McPherson et al.[73] were obtained with the same apparatus used in this experiment. Their data, extrapolated to threshold, give $a_0^+ = 21.5 \pm 0.9$ μb/sr. The ratio $R = a_0^-/a_0^+$ is therefore 1.27 ± 0.13 at threshold. This is in good agreement with our direct Coulomb-corrected values quoted above. From this we infer that $\Lambda/e = 0.06 \pm 0.7$, values also in agreement

with the above results.

The conclusions of these last few paragraphs are summarized in Table V. Our results demonstrate that detecting the ρ-exchange term near the photopion threshold through the minus-to-plus ratio R is a better method than considering either a_0^- or a_0^+ separately. The major conclusion of this work is that the dispersion theory of CGLN, modified by Ball, and the experimental results are in good agreement with a value of Λ/e consistent with zero. We also conclude that the Chew-Low extrapolation technique is a satisfactory one to apply to the deuteron for deriving reaction cross sections on free neutrons.

ACKNOWLEDGMENTS

The authors would like to express their sincere appreciation to Professor A. C. Helmholz for his continued encouragement and guidance throughout the course of this work. To Professor Geoffrey F. Chew and Dr. Michael J. Moravcsik we are grateful for several illuminating discussions of the results. We are grateful to Professor Roy L. Schult for providing us the method of Coulomb correction used. Thanks are due to Dr. Donald A. McPherson, who provided valuable help operating the chamber and in analyzing the results. Our appreciation goes to Mr. Richard I. Mitchell for his thorough programming of the kinematics analysis. To Mr. Rudin M. Johnson and the Synchrotron crew, we are indebted for many weeks of steady beam under unusual operating conditions. Thanks are due to Professor Luis W. Alvarez for the use of the bubble chamber and scanning equipment. Mr. Arnold J. Schwemin and Mr. Douglas Parmentier, Jr., provided valuable help with the chamber in earlier runs.

FOOTNOTES AND REFERENCES

* Work performed under the auspices of the U. S. Atomic Energy Commission.

† Present address: Department of Physics, University of Illinois, Urbana, Illinois

‡ Present address: Aerojet-General Nucleonics, San Ramon, California.

**Present address: Department of Physics, Case Institute of Technology, Cleveland, Ohio.

1. G. F. Chew, M. L. Goldberger, F. E. Low, and Y. Nambu, Phys. Rev. 106, 1345 (1957).

2. H. L. Anderson and E. Fermi, Phys. Rev. 86, 794 (1952).

3. H. P. Noyes, Phys. Rev. 101, 320 (1956).

4. J. M. Cassels, in Proceedings of the Seventh Annual Rochester Conference on High Energy Physics (Interscience Publishers, Inc., New York, 1957), II, p. 1.

5. G. Puppi, in Proceedings of the 1958 Annual International Conference on High Energy Physics at CERN (CERN, Geneva, 1958) 46-51.

6. M. J. Moravcsik, "The Low Energy Parameters of Pion Physics," paper in Proceedings of Eighth Annual International Conference on High Energy Physics, CERN (CERN, Geneva, 1958).

7. M. J. Moravcsik, Phys. Rev. 111, 1657 (1958).

8. J. Fischer, R. March, and L. Marshall, Phys. Rev. 109, 533 (1958).

9. A. M. Baldin, in Proceedings of the 1956 Annual Conference on High Energy Physics, CERN (CERN, Geneva, 1956) 272.

10. A. M. Baldin, Nuovo Cimento, Ser. 10, 8, 569 (1958).

11. A. M. Baldin and P. K. Kabir, Nuovo Cimento, Ser. 10, 9, 547 (1958).

12. M. Cini, R. Gatto, E. L. Goldwasser, and M. Ruderman, Nuovo Cimento, Ser. 10, 10, 243 (1958).

13. J. M. Cassels, Suppl. Nuovo Cimento, Ser. 10, 14, 259 (1959).

14. G. Bernardini, "Pion Photoproduction and Compton Effect on Nucleons," presented at Ninth International Annual Conference on High Energy Physics at Kiev, (Moscow 1960), Plenary Sessions I - V, 13.

15. J. Hamilton and W. S. Woolcock, Phys. Rev. 118, 291 (1960).

16. J. K. Walker, Nuovo Cimento, Ser. 10, 21, 577 (1961).

17. J. S. Ball, Phys. Rev. Letters 5, 73 (1960); Phys. Rev. 124, 2014 (1961).

18. M. Gourdin, D. Lurie, and A. Martin, Nuovo Cimento, Ser. 10, 18, 933 (1960).

19. B. DeTollis and A. Verganelakis, Nuovo Cimento, Ser. 10, 22, 406 (1961); B. DeTollis, E. Ferrari, and H. Munczek, Nuovo Cimento, Ser. 10, 18, 198 (1960).

20. P. Dennery, Phys. Rev. 124, 2000 (1961).

21. M. Kawaguchi, M. Miyamoto, and Y. Fujii, Nuovo Cimento, Ser. 10, 20, 408 (1961).

22. A. E. A. Warburton and M. Gourdin, Nuovo Cimento, Ser. 10, 22, 362 (1962).

23. J. M. McKinley, "Some Corrections to Partial Wave Dispersion Relations for Pion Photoproduction," University of Illinois Technical Report No. 38, (May 1962).

24. C. S. Robinson, P. M. Baum, L. Criegee, and J. M. McKinley, Phys. Rev. Letters 9, 349 (1962).

25. M. Gourdin and Ph. Salin, Nuovo Cimento, Ser. 10, 27, 193 (1963).

26. See, for example, W. R. Hogg, Proc. Phys. Soc. (London) 80, 729 (1962) for a review of data on the ratio R.

27. M. J. Moravcsik, Phys. Rev. 105, 267 (1957).

28. R. S. White, M. J. Jacobson, and A. G. Schultz, Phys. Rev. 88, 836 (1952).

29. M. Sands, J. G. Teasdale, and R. L. Walker, Phys. Rev. 95, 592 (1954).

30. M. Beneventano, D. Carlson-Lee, G. Stoppini, G. Bernardini, and E. L. Goldwasser, Nuovo Cimento, Ser. 10, 12, 156 (1954).

31. D. Carlson-Lee, G. Stoppini, and L. Tau, Nuovo Cimento, Ser. 10, 2, 162 (1955).

32. M. Beneventano, G. Stoppini, L. Tau, and G. Bernardini, in Proceedings of the CERN Symposium on High Energy Accelerators and Pion Physics, Geneva (CERN, Geneva, 1956) II, p. 259.

33. M. I. Adamovich, V. I. Veksler, G. V. Kuzmicheva, V. G. Larionova, and S. P. Kharlamov, in Proceedings of the CERN Symposium on High Energy Accelerators and Pion Physics, Geneva(CERN, Geneva, 1956) II, 265.

34. K. M. Watson, J. C. Keck, A. V. Tollestrup, and R. L. Walker, Phys. Rev. 101, 1159 (1956).

35. M. Beneventano, G. Bernardini, D. Carlson-Lee, G. Stoppini, and L. Tau, Nuovo Cimento, Ser. 10, 4, 323 (1956).

36. M. J. Moravcsik, Nuovo Cimento, Ser. 10, 7, 442 (1958).

37. M. Beneventano, G. Bernardini, G. Stoppini, and L. Tau, Nuovo Cimento, Ser. 10, 10, 1109 (1958).

38. D. Carlson-Lee, Bull. Am. Phys. Soc., Ser. II, 3, 334 (1958), and private communication.

39. S. P. Kharlamov, M. I. Adamovich, , and V. G. Larionova, Zh. Eksperim. i Teor. Fiz. 36 945 (1959), translated in Soviet Phys.-JETP 9, 668 (1959).

40. W. R. Hogg and E. H. Bellamy, Proc. Phys. Soc. (London) 72, 895 (1958).

41. M. I. Adamovich, G. V. Kuz'micheva, V. G. Larionova, and S. P. Kharlamov, Zh. Eksperim. i Teor. Fiz. 35, 27 (1958), translated in Soviet Phys.-JETP 8, 21 (1959).

42. M. I. Adamovich, Zh. Eksperim. i Teor. Fiz. 35, 39 (1958), translated in Soviet Phys.-JETP 8, 29 (1959).

43. J. G. Rutherglen and J. K. Walker, Proc. Phys. Soc. (London) 76, 430 (1960).

44. J. P. Burq and J. K. Walker, Phys. Rev. 132, 447 (1963).

45. J. Pine and M. Bazin, Phys. Rev. 132, 2735 (1963).

46. G. Gatti, P. Hillman, W. C. Middelkoop, T. Yamagata, and B. Zavattini, Phys. Rev. Letters 6, 706 (1961).

47. Roy L. Schult (University of Illinois, Urbana, Illinois) private communication, 1963.

48. G. F. Chew and F. E. Low, Phys. Rev. 113, 1640 (1959).

49. D. Parmentier, Jr., and A. J. Schwemin, Rev. Sci. Instr. 26, 954 (1955).

50. Harry C. Dittler and Thomas F. Gerecke, Liquid Hydrogen Bubble Chambers (M. S. Thesis), UCRL-2985, May 1955.

51. D. C. Gates, R. W. Kenney, D. A. McPherson, and W. P. Swanson, Rev. Sci. Instr. 31, 565 (1960).

52. D. C. Gates, R. W. Kenney, and W. P. Swanson, Phys. Rev. 125, 1310 (1962).

53. William P. Swanson, Photopion Production from Deuterium near Threshold (Ph.D. Thesis), Lawrence Radiation Laboratory Report UCRL-9194, 1960.

54. F. J. Loeffler, T. R. Palfrey, and G. W. Tautfest, Nucl. Instr. Meth. 5, 50 (1959).

55. J. W. DeWire (Cornell University, Ithaca, N. Y.) "Calibration Data for the Quantameter and the Cornell Thick-Walled Ionization Chamber, private communication, November 1959.

56. G. Clark and W. F. Diehl, "Range-Energy Relation for Liquid Hydrogen Bubble Chambers," Lawrence Radiation Laboratory Report UCRL-3789, May 1957.

57. W. E. Deming, Statistical Adjustment of Data (John Wiley and Sons, Inc., New York, 1943), Chapter 4.

58. J. Peter Berge, Frank T. Solmitz, and Horace D. Taft, Rev. Sci. Instr. 32, 538 (1961).

59. Michael J. Moravcsik, Phys. Rev. 114, 621 (1959).

60. L. Hulthén and M. Sugawara, "The Two-Nucleon Problem," Encyclopedia of Physics, (Springer-Verlag, Berlin, 1957) 39, p.1.

61. G. Bernardini and E. L. Goldwasser, Phys. Rev. 94, 729 (1954); Phys. Rev. 95, 857 (1954).

62. J. E. Leiss, C. S. Robinson, and S. Penner, Phys. Rev. 98, 201 (1955).

63. G. M. Lewis and R. E. Azuma, Proc. Phys. Soc. (London) 73, 873 (1959).

64. A. Barbaro, E. L. Goldwasser, and D. Carlson-Lee, Bull. Am. Phys. Soc. 4, 23 (1959).

65. J. E. Leiss, S. Penner, and C. S. Robinson, results reported in reference 14.

66. J. G. Rutherglen and J. K. Walker, Proc. Phys. Soc. 76, 430 (1960).

67. M. I. Adamovich, E. G. Gorzhevskaja, S. P. Kharlamov, V. G. Larionova, V. M. Popova, and F. Yagudina in A. M. Baldin, "Relativistic Dispersion Approach to Pion Photoproduction near Threshold," in Proceedings of the 1960 Annual International Conference on High Energy Physics at Rochester (Interscience Publishers, New York, 1960), p. 330.

68. J. K. Walker and J. P. Burq, Phys. Rev. Letters 8, 37 (1962).

69. J. K. Walker, J. G. Rutherglen, D. B. Miller, and J. M. Paterson, Proc. Phys. Soc. (London) 81, 78 (1963).

70. R. A. Carrigan and E. L. Goldwasser, Photoproduction of Positive Pions from Hydrogen near Threshold, Technical Report No. 32, University of Illinois (1962).

71. G. M. Lewis, R. E. Azuma, E. Gabathuler, D. W. G. S. Leith, and W. R. Hogg, Phys. Rev. 125, 378 (1962).

72. M. J. Bazin and J. Pine, Phys. Rev. 132, 830 (1963).

73. D. A. McPherson, D. C. Gates, R. W. Kenney, and W. P. Swanson, Positive Photopion Production from Hydrogen near Threshold (to be published in Phys. Rev.)

74. J. Orear, Notes on Statistics for Physicists, Lawrence Radiation Laboratory Report UCRL-8417, 1958.

75. Leonard B. Auerbach, Tom Eliof, William B. Johnson, Joseph Lach, Clyde E. Wiegand, and Thomas Ypsilantis, Phys. Rev. Letters 9, 173 (1962).

76. Preliminary results were reported in W. P. Swanson, D. C. Gates, T. L. Jenkins, and R. W. Kenney, Phys. Rev. Letters 5, 336 (1960).

77. Preliminary results were reported in W. P. Swanson, D. C. Gates, T. L. Jenkins, and R. W. Kenney, Phys. Rev. Letters 5, 339 (1960).

78. James D. Simpson, (Department of Physics, University of Illinois, Urbana, Illinois) private communication (1964). The s-wave phase shifts "Set X" of Ref. 23, and p-wave phase shifts from the effective range formula of CGLN were used to calculate $N^{(-)}$. The large error assigned to $N^{(-)}$ is an estimated uncertainty due to uncertainties in the choice of S-wave phase shifts.

Table I. Analysis and results of the minus-to-plus ratio.

Bin description			Negative pions						Positive pions			Results*	
Bin number	Photon energy (lab) (nominal) (MeV)	Pion angle (c.m.) (nominal) (deg)	Average photon energy (lab) (MeV)	Raw number seen	Coulomb correction factor p-p	Coulomb correction factor π^--p	Geometry correction factor	Corrected number	Raw number seen	Geometry correction factor	Corrected number	R as a function of k (lab)	R (averaged)
I A	152-155	0-60	161	10	1.06	0.79	1.04	8.7	16	1.056	16.9	> 0.79	
B		60-90	159	16	1.04	0.82	1.03	14.1	13	1.021	13.3	$\pm$ 0.21	
C		90-105	160	2	1.05	0.83	1.04	1.7	1	1.000	1.0		
II A	155-157.5	0-60	160	13	1.03	0.86	1.21	13.9	3	1.296	3.9	> 1.35	> 1.13
B		60-90	160	24	1.11	0.86	1.09	25.0	16	1.108	17.7	$\pm$ 0.26	$\pm$ 0.13
C		90-105	159	15	1.05	0.83	1.03	13.5	7	1.011	7.1		
D		105-120	159	12	1.05	0.83	1.03	10.8	18	1.001	18.0		
IIIA	157.5-162.5	60-90	161	30	1.06	0.88	1.19	33.3	15	1.403	21.0	> 1.13	
B		90-105	164	26	1.03	0.88	1.15	27.1	23	1.127	25.9	$\pm$ 0.21	
C		105-120	161	10	1.06	0.86	1.10	10.0	15	1.013	15.2		
D		105-120	163	21	1.05	0.87	1.10	21.1	13	1.117	14.5	1.22	
E		120-135	163	22	1.10	0.86	1.14	23.7	18	1.005	18.1	$\pm$ 0.25	
F		135-150	159	8	1.12	0.86	1.11	8.6	11	1.001	11.0		
IV A	162.5-167.5	105-120	162	24	1.08	0.89	1.30	30.0	9	1.954	17.6	1.38	
B		120-135	166	36	1.05	0.89	1.19	40.0	28	1.180	33.0	$\pm$ 0.21	
C		135-150	166	29	1.04	0.88	1.18	31.3	23	1.037	23.9		1.28
D		150-180	162	23	1.06	0.87	1.12	23.8	16	1.016	16.3		$\pm$ 0.13
V A	167.5-172.5	135-150	166	31	1.08	0.89	1.36	40.5	22	1.451	31.9	1.04	
B		150-180	165	13	1.11	0.89	1.30	16.7	20	1.153	23.1	$\pm$ 0.22	
VI A	172.5-175	150-180	170	11	1.23	0.91	1.18	14.5	4	1.398	5.6	2.60 $\pm$ 1.52	

*The results are the corrected number of negative pions divided by the corrected number of positive pions, times a correction factor (1.056±0.03) explained in the text.

-36-

UCRL-11587

Table II. Parameters used in the Chew-Low extrapolation. Pion units ($\hbar = c = \mu = 1$) are used, except where noted.

Symbol	Definition	Value
p_1	Momentum of spectator proton	--
p_2	Momentum of parent nucleon	--
w	Invariant energy of $\pi^- p$ system	--
w_0	$(M_p + \mu)$, threshold value of w	7.7212
k	Energy (lab) of synchrotron photon (Mev)	--
k_t	Threshold value of k (MeV)	145.8
α^2	Inverse deuteron radius, squared	0.107
Γ^2	$(4/M_p)(\alpha/(1 - \alpha r_{0t}))$	0.3217
B.E.	Deuteron binding energy	2.225 MeV
M_d	Deuteron mass	13.436
M_p	Proton mass	6.7212
M_n^2	Neutron mass squared	45.30
r_{0t}	Triplet np effective range	$(1.702 \pm 0.029) \times 10^{-13}$ cm.
μ	Pion mass	1.0
$k_{\gamma n}$	Photon energy (lab) in reaction $\gamma n \rightarrow \pi^- p$ (Mev)	--
W	Phase-space factor	--
p_π^*	Pion momentum (c.m.) in reaction $\gamma n \rightarrow \pi^- p$	--
ω	Pion full energy (c.m.) in reaction $\gamma n \rightarrow \pi^- p$	--
ν	Photon momentum (c.m.) in reaction $\gamma n \rightarrow \pi^- p$	--
E_i	Nucleon initial energy (c.m.) in reaction $\gamma n \rightarrow \pi^- p$	--
E_f	Nucleon final energy (c.m.) in reaction $\gamma n \rightarrow \pi^- p$	--
$S(k)$	Synchrotron photon spectrum, photons/MeV	--
C_c	Coulomb correction for final state	--
E	Geometrical detection efficiency	--
N	Deuterons per cubic centimeter $= N_0 \rho / A$	0.3908×10^{23} cm^{-3}
t	Target thickness available	7.0 cm
N_0	Avogadro's number	6.025×10^{23}
ρ	Density of liquid deuterium	0.1307 gm/cm^3
A	Deuteron mass, AMU	2.015

Table III. Results of the Chew-Low extrapolation

Parameter	Table A	Table B	Table A + B
A_0 (μb/sr)	27.0 ±4.0	0.34±2.2	25.85±2.6
A_1 (μb/sr)	- 2.67±2.4	- 5.72±1.2	- 2.93±1.6
A_2 (μb/sr)	- 2.8 ±2.3	1.32±0.82	- 0.58±0.9
A_3 (μb/sr-MeV)	0.14±0.07	0.23±0.03	- 0.005±0.04
A_4 (μb/sr)	- 2.30±1.6	6.52±0.76	0.18±0.86
$da_0^-/dk_{\gamma n}$ (μb/sr-Mev)	- 0.26±0.23	-	- 0.28±0.16
$\ell n\, \mathcal{L}$	1017.8	792.3	2131.1

The parameters are defined by Eq. (8). A_0 is the experimental threshold value of a_0^- in units of μb/sr. Experimental values of the slope $da_0^-/dk_{\gamma n} = 2\, A_1\, M_n$ are given in units of (μb/sr-Mev). Differences between the various results in Table III are explained in the text. Errors are statistical only and were obtained from the error matrix defined in the text. A_0 and A_1 are subject to a correction factor (1.056±0.030) explained in Sec. III. C, and an additional normalization uncertainty of ± 4%.

Table IV. Error matrix $G_{ij} = \langle \Delta A_i \, \Delta A_j \rangle$ of the parameters for Table A + B.

Index	0	1	2	3	4
0	6.750	- 3.162	- 1.811	0.026	0.644
1	- 3.162	2.492	1.043	- 0.0018	- 1.002
2	- 1.811	1.043	0.769	- 0.017	- 0.324
3	0.026	- 0.0018	- 0.017	0.0018	- 0.017
4	0.644	- 1.002	- 0.324	- 0.017	0.7450

This table includes statistical errors only.

Table V. Derived values for Λ/e.

Experimental quantity	Assumptions	Derived value Λ/e
$R = 1.28 \pm 0.13$ 160 MeV $< k <$ 175 MeV $\theta^* > 110$ deg	$R = 1.28\,(1 - 0.14\Lambda)$ [a]	$\Lambda/e = 0.0 \pm 0.7$
$R \geq 1.13 \pm 0.13$ 152 MeV $< k <$ 160 MeV $\theta^* < 110$ deg	$R = 1.28\,(1 - 0.14\Lambda)$ [a]	$\Lambda/e \leq 0.8 \pm 0.7$
$a_0^- = (27.3 \pm 2.8)$ μb/sr at threshold	$N^{(-)} = 0.04 \pm 0.04$ [b] $f^2 = 0.08$	$\Lambda/e = 1.9 \pm 1.8$
$a_0^- = (27.3 \pm 2.8)$ μb/sr $a_0^+ = (21.5 \pm 0.9)$ μb/sr [c] at threshold	$R = 1.28\,(1 - 0.14\,\Lambda)$ [a] $= 1.27 \pm 0.13$	$\Lambda/e = 0.06 \pm 0.7$

[a] Ref. 17. [b] Ref. 78. [c] Ref. 73.

FIGURE CAPTIONS

Fig. 1. Schematic diagram of setup. The internal electron beam of the synchrotron produces a bremsstrahlung beam of peak energy 194 MeV. The beam is first collimated and swept, and then hardened by approximately one radiation length of LiH before entering the 4-in. deuterium bubble chamber.

Fig. 2. An example of the reaction $\gamma d \rightarrow \pi^- 2p$ in the 4-in. deuterium bubble chamber. Beam enters at the top of the picture. The pion is the light track going to the reader's left and forward.

Fig. 3. An example of the reaction sequence $\gamma d \rightarrow \pi^+ 2n$, $\pi^+ \rightarrow \mu^+ \nu$, seen in the 4-in. deuterium bubble chamber. Positive pions are normally identified by their muon decay. In 26% of the cases, the positron track is also visible. Beam enters at top of picture. The pion is seen in the upper right, and the decay muon is near the fiducial crosses.

Fig. 4. Laboratory energy and angle bins used to determine R.

Fig. 5. Distribution of true laboratory photon energy for the reaction $\gamma d \rightarrow \pi^- 2p$ about the energy given by two-body kinematics. The three histograms are explained in the text. Momentum (lab) in MeV/c and angle bins accepted:

	a	b	c
$29 < P_\pi < 37$,	$0.0 < \cos\theta_\pi$	$-0.7 < \cos\theta_\pi < 0.0$	$\cos\theta_\pi < -0.7$
$37 < P_\pi < 44$,	$0.3 < \cos\theta_\pi$	$-0.3 < \cos\theta_\pi < 0.3$	$\cos\theta_\pi < -0.3$
$44 < P_\pi < 51$,	$0.7 < \cos\theta_\pi$	$0.0 < \cos\theta_\pi < 0.7$	$\cos\theta_\pi < 0.0$

Fig. 6. Pology diagram showing kinematically allowed regions of the variables p_1^2 and w^2 (pion units). The variable p_1^2 is the square of the spectator proton's momentum, and w^2 is the square of the total energy of the other proton and pion in their center of mass. The shaded areas are kinematic regions actually used

Fig. 6 (cont'd) in this experiment, where corrections to the data could be reliably made. Experimental cross sections are to be extrapolated to $p_1^2 = -\alpha^2 = -0.107$.

Fig. 7. Graphs of $\ell n \mathcal{L}$ versus each parameter A_i, for results of Table A + B (see Sec. IV.A).

Fig. 8. Variation of the matrix element squared a_0^- with laboratory-system photon energy $k_{\gamma n}$. The solid curves are from the theory of CGLN ($f^2 = 0.08$). The solid line is our determination of a_0^- by means of a Chew-Low extrapolation, corrected by the Coulomb penetration factor. It includes the correction factor (1.056 ± 0.03). The dashed lines indicate confidence limits on our results. They take into account a 3% uncertainty in the correction factor, and a 4% uncertainty in the beam monitor calibration.

Fig. 9. The minus-to-plus ratio R, corrected for final-state Coulomb interactions, compared with the predictions of the dispersion relations of CGLN, for various c.m. angles. The curves are from the paper of Beneventano et al. (reference 37). Two-body kinematics were used to determine the laboratory photon energy and pion angle. Where noted by "our correction," we have made Coulomb corrections to the experimental results of others by interpolating the corrections obtained in Table I.

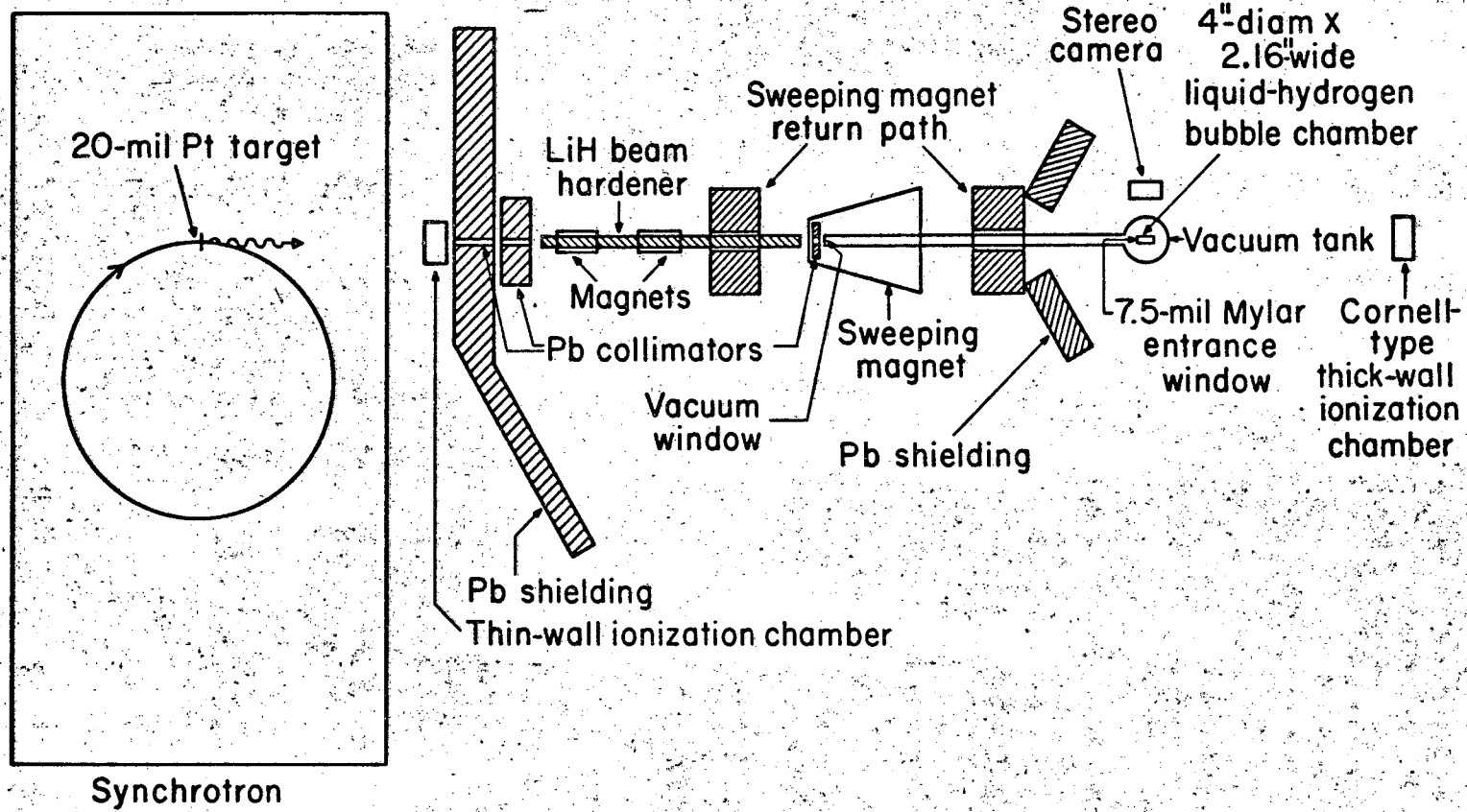

Fig. 1.

UCRL-11587

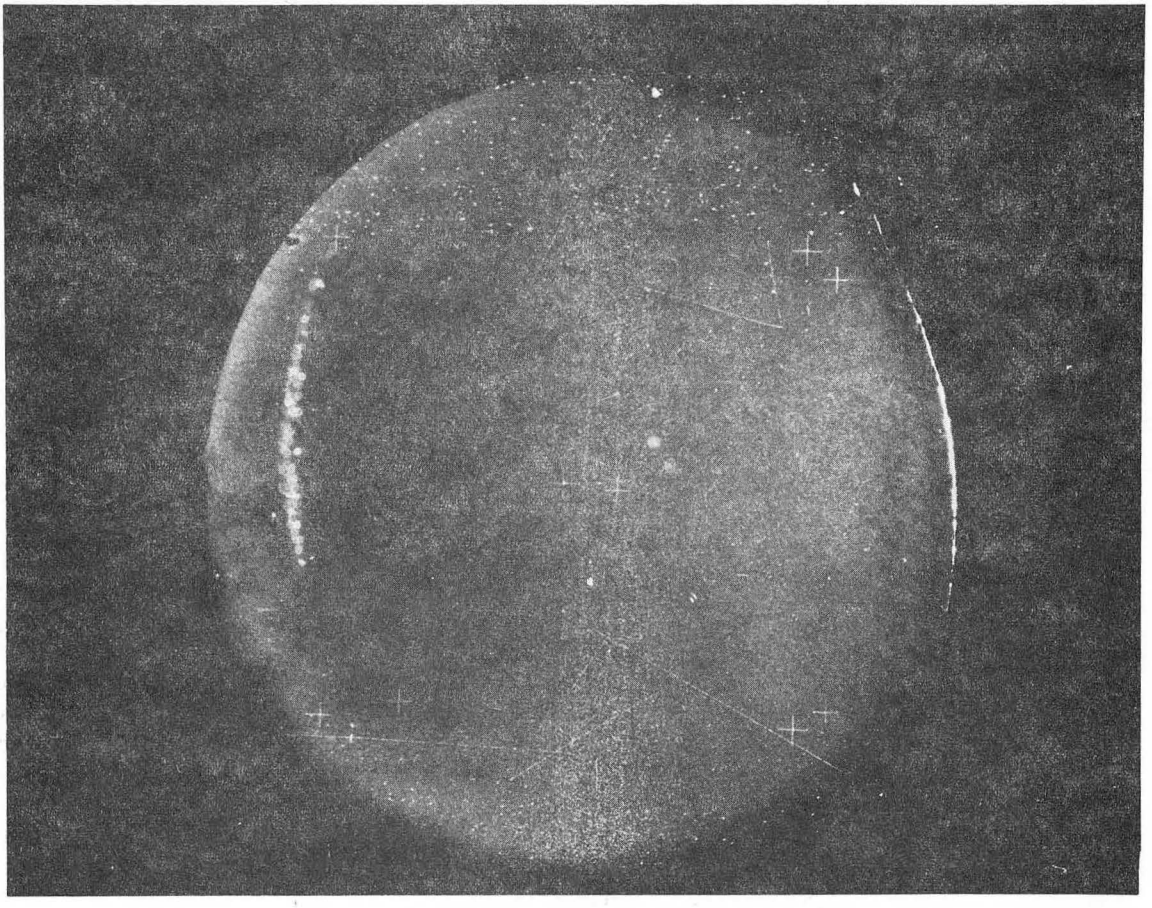

ZN-4494

Fig. 2

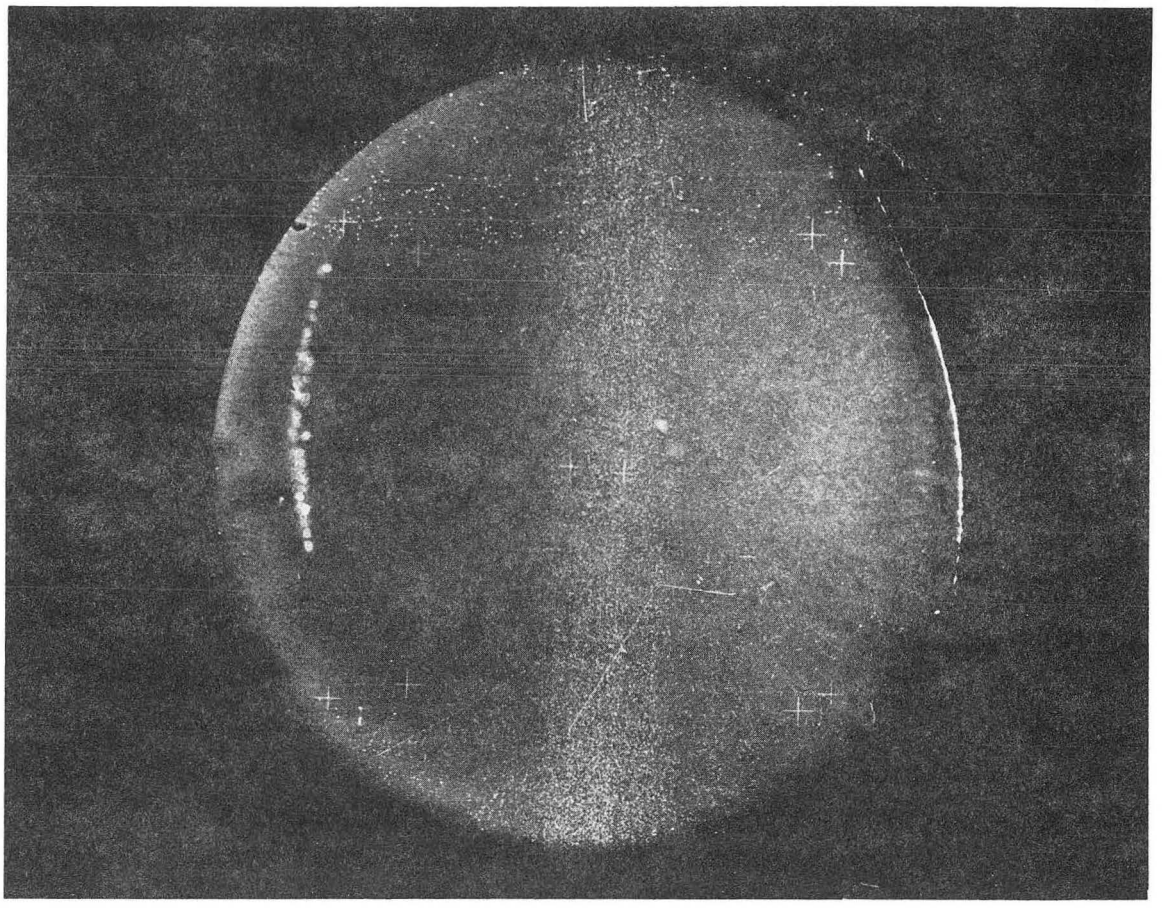

ZN-4493

Fig. 3

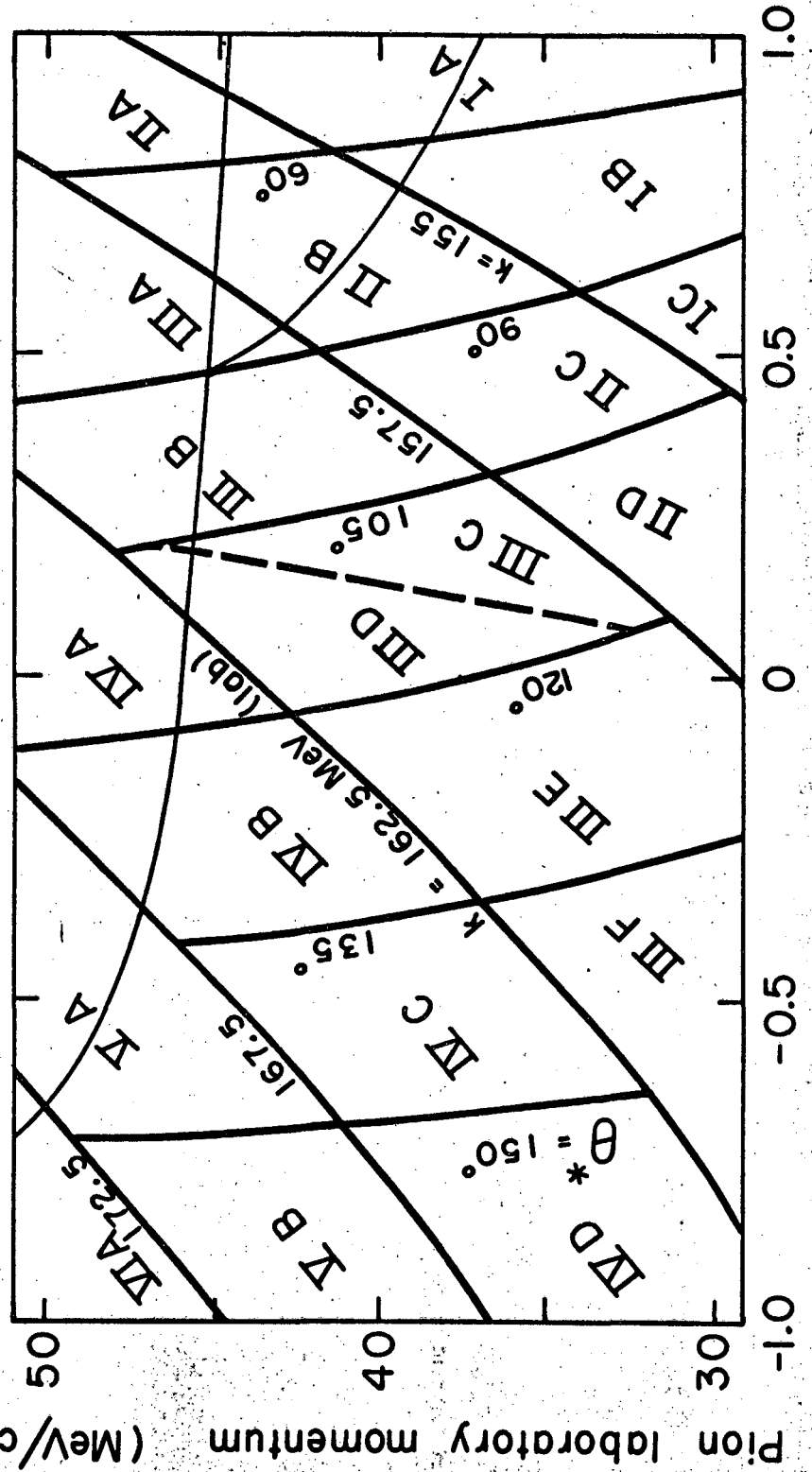

MU-33434

Fig. 4.

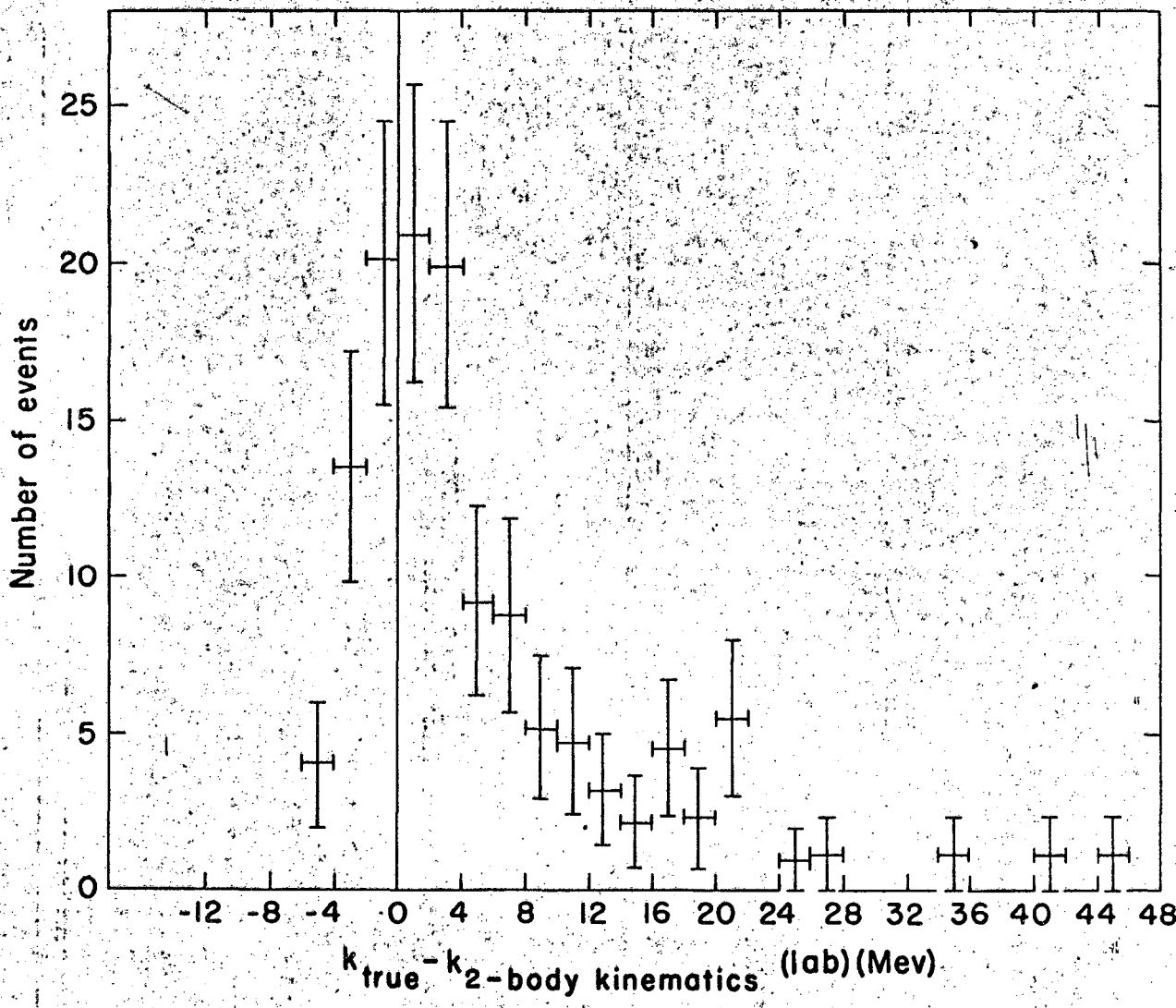

MUB-3745

Fig. 5(a).

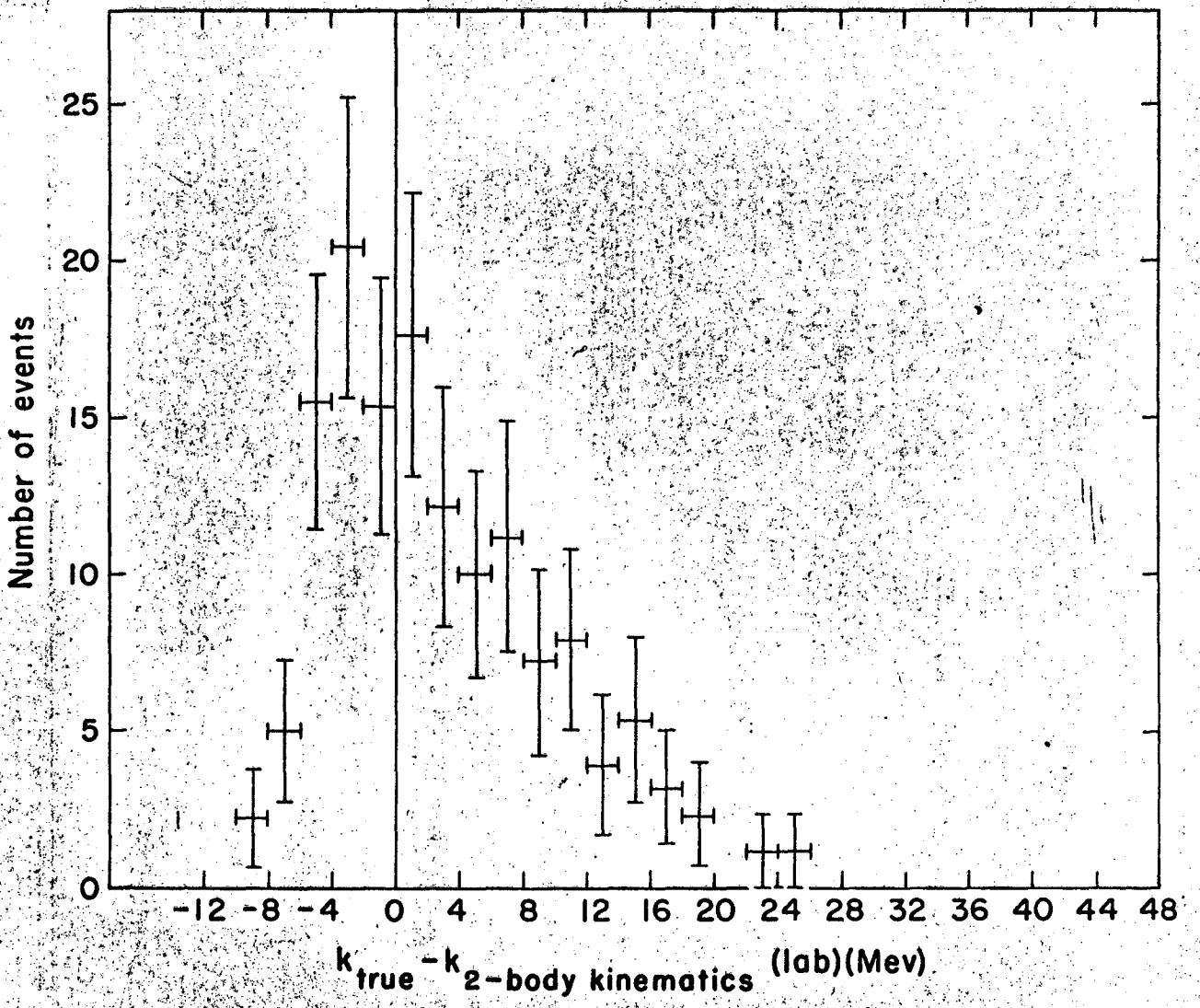

MUB-3746

Fig. 5(b)

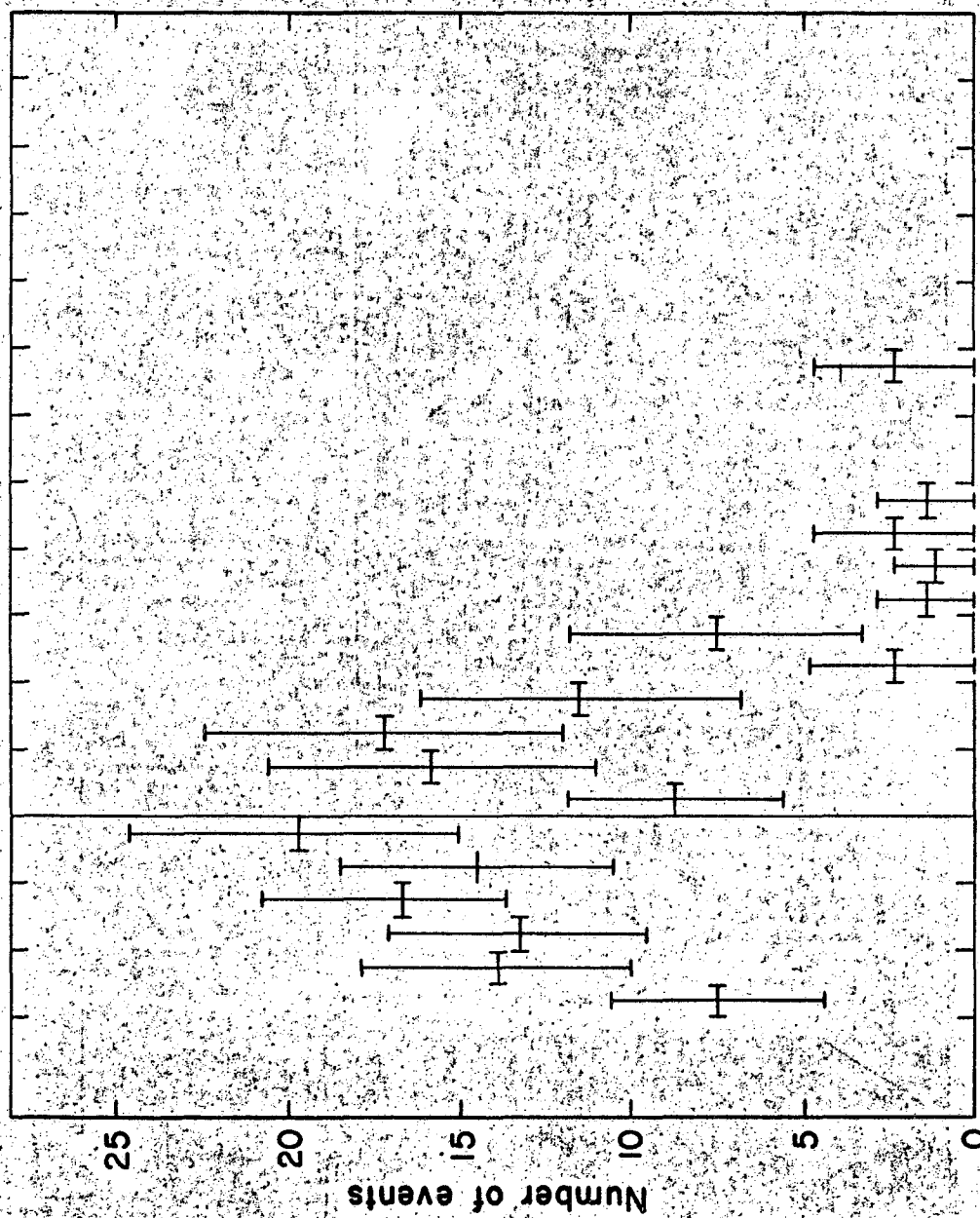
Number of events
0
5
10
15
20
25
-12
-8
-4
0
4
8
12
16
20
24
28
32
36
40
44
48
$k_{true} - k_{2-body}$ kinematics (lab) (Mev)
MUB-3747

Fig. 5(c).

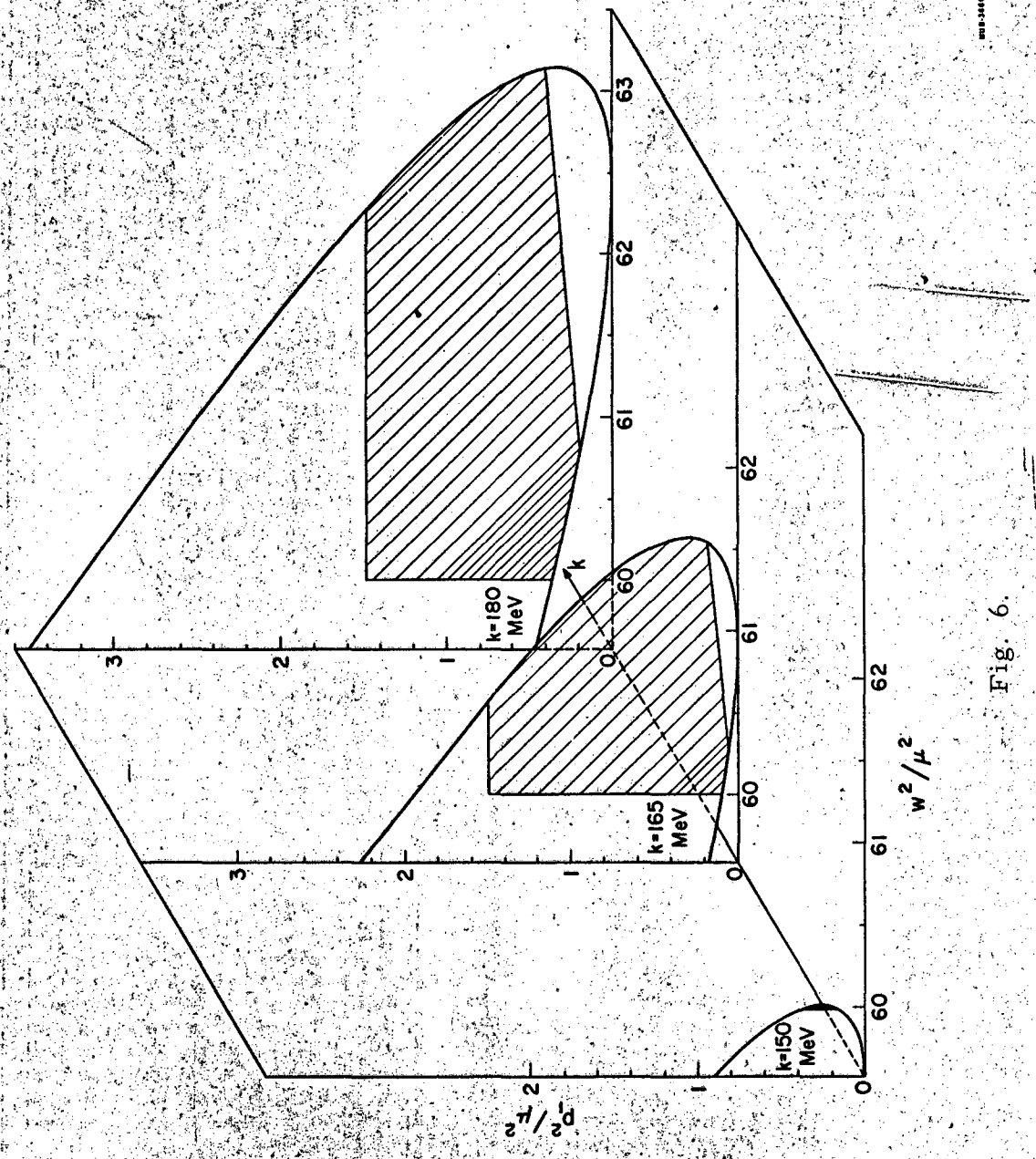

Fig. 6.

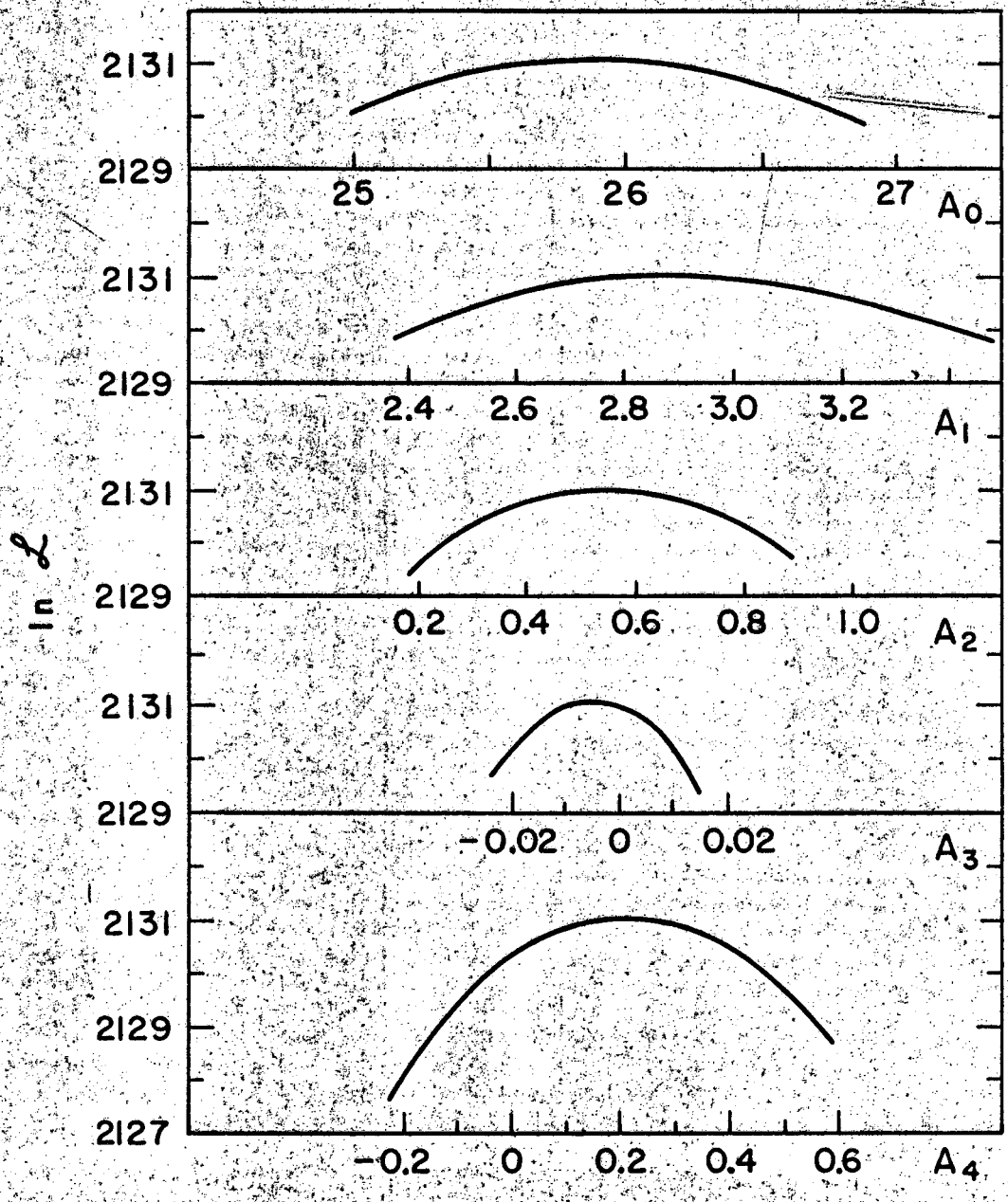
2131
2129
25
26
27
A_0
2131
2129
2.4
2.6
2.8
3.0
3.2
A_1
2131
2129
0.2
0.4
0.6
0.8
1.0
A_2
2131
2129
-0.02
0
0.02
A_3
2131
2129
2127
-0.2
0
0.2
0.4
0.6
A_4
χ^2
MUB-3744

Fig. 7

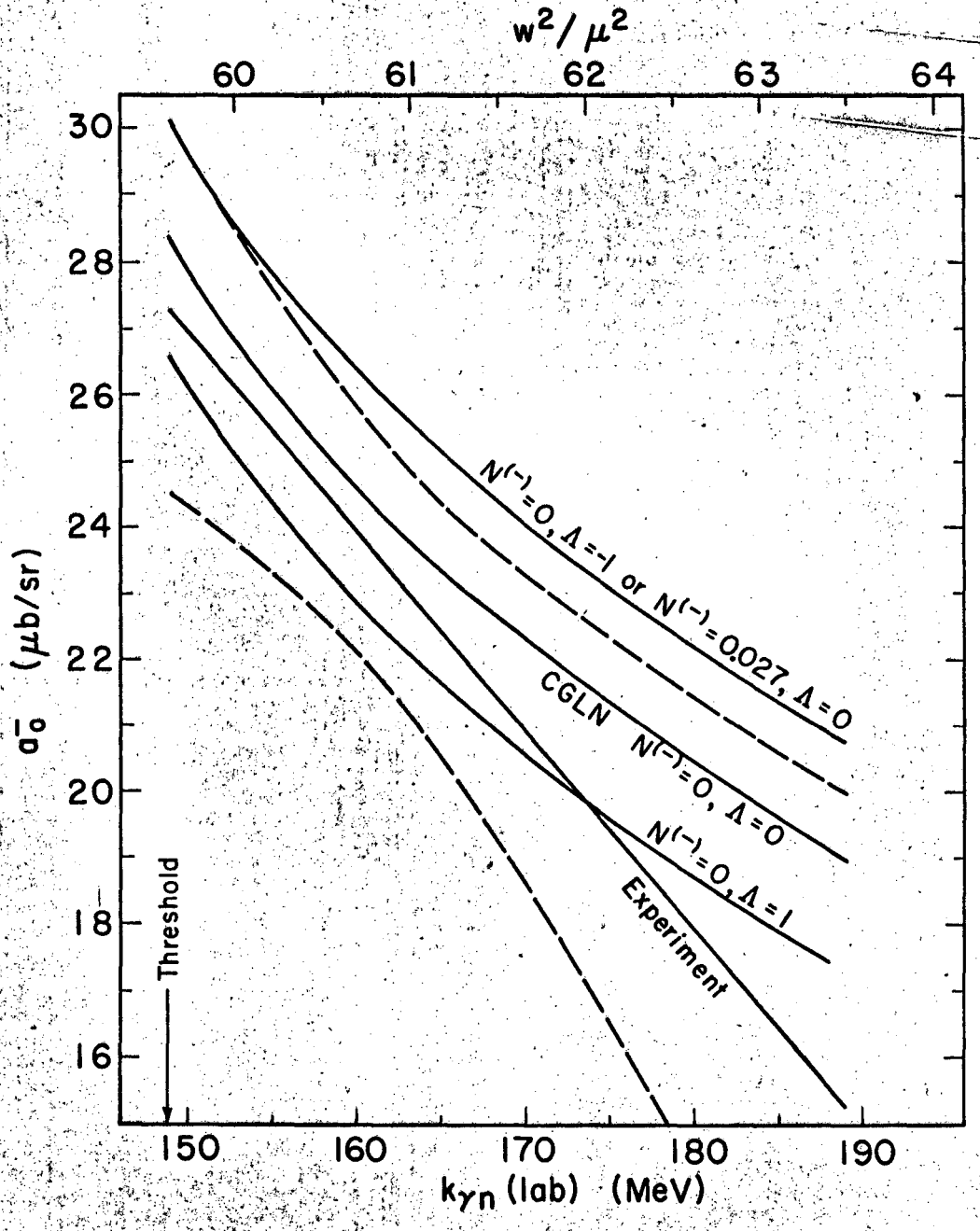
w^2/μ^2
60
61
62
63
64
30
28
26
24
22
20
18
16
$a\bar{o}$ (μb/sr)
$N^{(-)}=0, \Lambda=-1$ or $N^{(-)}=0.027, \Lambda=0$
CGLN $N^{(-)}=0, \Lambda=0$
$N^{(-)}=0, \Lambda=1$
Experiment
Threshold
150
160
170
180
190
$k_{\gamma n}$ (lab) (MeV)
MUB-3758

Fig. 8

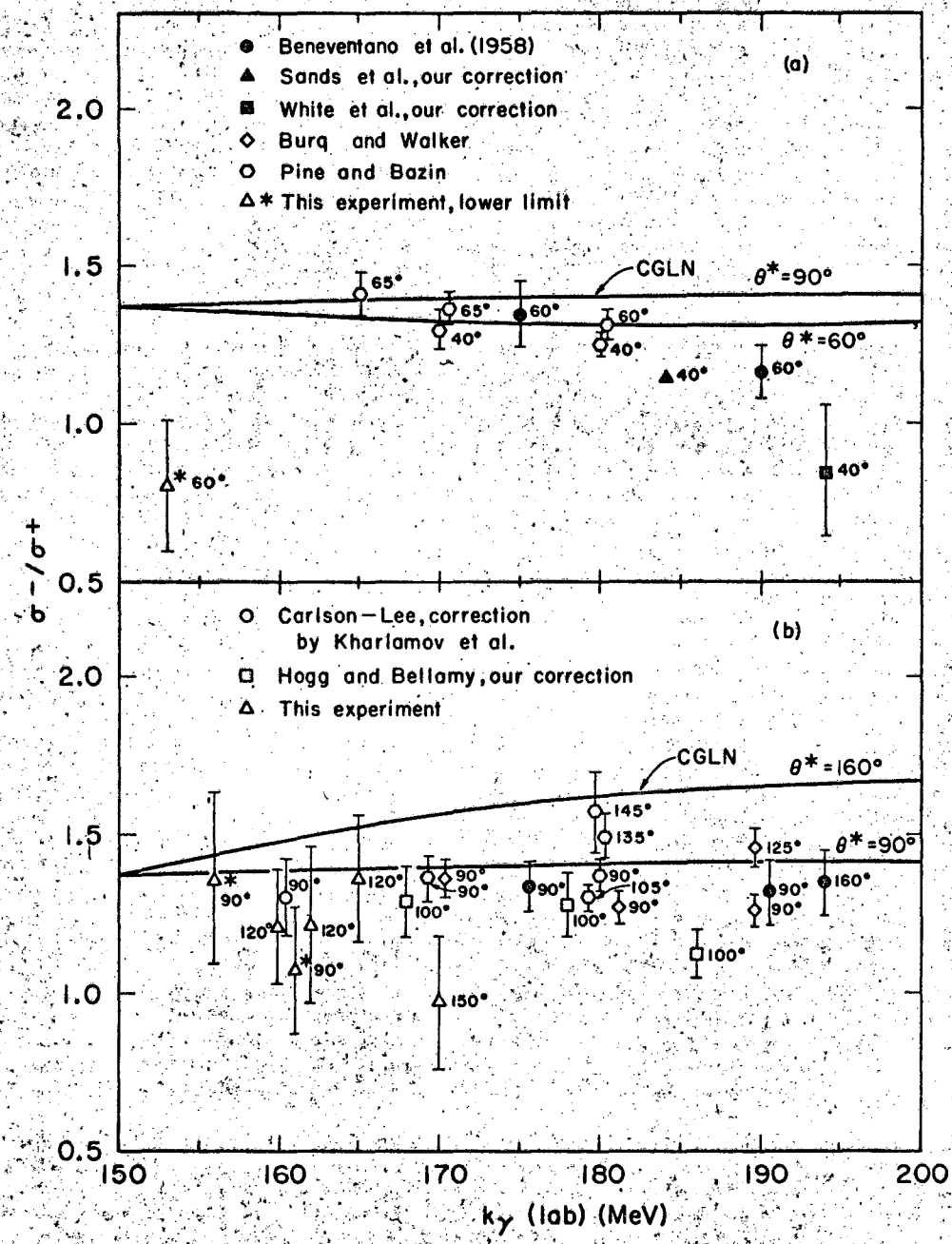
Beneventano et al. (1958)
Sands et al., our correction
White et al., our correction
Burq and Walker
Pine and Bazin
This experiment, lower limit
(a)
CGLN
θ*=90°
θ*=60°
65°
60°
40°
Carlson–Lee, correction by Kharlamov et al.
Hogg and Bellamy, our correction
This experiment
(b)
CGLN
θ*=160°
θ*=90°
145°
135°
125°
160°
105°
150°
σ− / σ+
2.0
1.5
1.0
0.5
150
160
170
180
190
200
kγ (lab) (MeV)
MUB-3748

Fig. 9